University of Groningen
Kapteyn Astronomical Institute

Bachelor Thesis

Astronomy

Improving the Kapteyn Radio Telescope

Author:
Job Formsma
S2758717

Supervisors:
Prof. Dr. A (Andrey) Baryshev
Dr. R. (Ronald) Hesper

July 18th, 2017

Abstract

This project was based around reworking and upgrading the Kapteyn Radio Telescope (KRT) with the primary objective to measure the temperature of the Comic Microwave Background (CMB). Previous observations of the CMB with the KRT showed a negative value for its temperature. By rebuilding the frame of the telescope and replacing the cold load, the calibration showed a major improvement. Also the receiver of the system is replaced with a Low-Noise Block downconverter, which decreased the receiver noise by a factor two. Observations were done with the telescope to see if applied upgrades yielded better results. Measurements of the CMB temperature showed a temperature of 2.90 $\pm$ 1.11 Kelvin.

Contents

1 Introduction

1.1 Radio Astronomy

Almost everything we know about the universe has been obtained with observations of electromagnetic radiation[1]. This ranges from signals of high energy gamma rays to low energy radiation such as radio waves. In the field of radio astronomy celestial objects are studied at frequencies radio frequencies ranging from approximately 10 MHz to 1 THz.

The first astronomical radio observation was, by accident, done by Karl Jansky in 1931. To investigate static that interfered with voice transmissions, he used a rotating array of antennas which let him observe the whole sky (see Fig. 1a). After recording signals for multiple months, Jansky could categorize three different signals. From nearby thunderstorms, from far away thunderstorms and a signal he could not explain. After a year of studying the signal he determined that the signal came from the Milky Way.

In less than 100 years we have made a lot of progress in the field of radio astronomy. Big telescope arrays such as the Atacama Large Millimeter Array (ALMA) or the Low Frequency Array (LOFAR) use interferometry for better resolution and imaging. With the field of radio astronomy we have gained a lot of new knowledge about the current and old universe with its interesting objects in it. Objects such as active galactic nuclei and the galactic center of the Milky Way can be seen in the radio regime and their interesting properties can be studied.

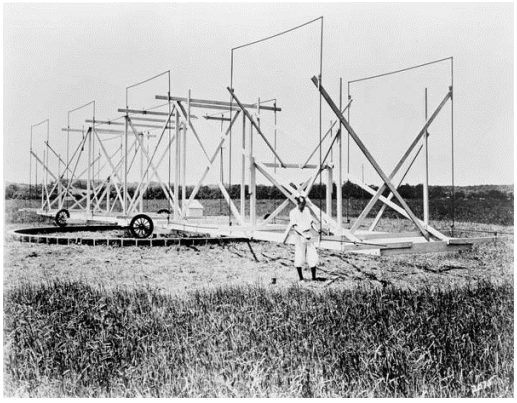

(a) Karl Jansky with his antenna array.

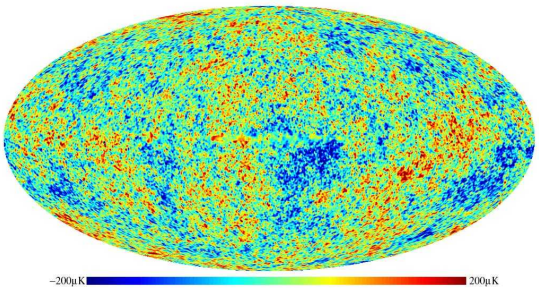

(b) WMAP picture of the Cosmic Microwave Background

Figure 1: Radio Astronomy Introduction

1.2 Cosmic Microwave Background Radiation

The Cosmic Microwave Background (CMB) is radiation from the hot and dense early universe. In the first thousands of years after the Big Bang the universe was so hot that photons were trapped by the free protons and electrons floating in the plasma due to Thomson scattering. After approximately 380000 years the universe had, due to expansion, cooled down enough for the protons and electrons to combine. In this *epoch of recombination* the universe became transparent in which the photons do not get scattered anymore. The photons could freely travel through the universe.

[1]The rest by: Neutrinos, Cosmic Rays and Gravitational waves

Those photons are that of a black body following Planck's Law (see equation (1)). At the time of recombination the universe was about 3000 Kelvin, which is the temperature at which all hydrogen is neutral. The radiation of that corresponding black body curve is redshifted to todays value due to expansion of the universe. The CMB has a black body spectrum following Plancks Law at a temperature of 2.72548 ± 0.00057 Kelvin [Fixsen, 2009]. This corresponds to a maximum intensity at approximately a wavelength of 1mm. In Figure 1b the whole sky image of the CMB radiation is shown. The picture is made by the Wilkinson Microwave Anisotropy Probe (WMAP). In the picture we can see that the intensity of the CMB is not completely uniform. The intensity differences are due to quantum fluctuations and clustering of matter in the early universe. However, the CMB is still the most perfect black-body spectrum ever seen in nature [White, 1999].

The existence of the CMB was first predicted in 1948 by Ralph Alpher and Robert Herman [Alpher and Herman, 1948]. They estimated the temperature of such a background radiation to be around 5 Kelvin. First observations of the CMB were done by Arno Penzias and Robert Wilson in 1964. With their big horn antenna they measured an excess antenna temperature in their equipment which they could not account for [Penzias and Wilson, 1965]. An isotropic signal of 3.5 Kelvin was measured in their observations.

2 Radio Astronomy Basics

In the field of radio astronomy we observe in the radio regime. This is electromagnetic radiation with a frequency of roughly 10 MHz to 1 THz. Observing sources in the sky can be done from the ground, in the air or from space. Radiation up to 200 GHz can easily pass through the atmosphere of the Earth, making radio astronomy an excellent method of observing with ground based observatories.

Before we can observe the CMB and determine its temperature, a few basic definitions that are used in radio astronomy have to be introduced.

2.1 Black Body Radiation

Black-body radiation is radiation coming from an object of which the frequency spectrum of the radiation is completely dependent on the body's temperature. This is called the Planck's spectrum, which is the spectrum of the radiation emitted following the Plank's Law

$$B_\nu(T) = \frac{2h\nu^3}{c^2} \frac{1}{e^{h\nu/k_B T} - 1} \ , \tag{1}$$

where h is the Plancks constant, k_B is the Boltzmann constant, c is the speed of light, ν is the frequency of interest and T the temperature of the black-body. The spectrum has a maximum at a specific frequency matching the temperature of the body which follows Wien's displacement law. At room temperature most of the radiation is in the infrared, which humans can not see, but for example the Sun is a lot hotter at its surface with an effective temperature of 5800 Kelvin. This higher temperature corresponds to a higher frequency peak of 600 THz, making the Sun visible to the eye.

In the epoch of recombination, when the CMB radiation was formed, the universe had a uniform temperature of approximately 3000 Kelvin. The radiation of the CMB that formed is that of a Planck's spectrum of a black-body with a temperature of 3000 Kelvin. Due to the expansion of the universe this spectrum is shifted towards today's value of 2.73 Kelvin. The spectrum of this radiation is still the spectrum following Planck's Law, but now for a different temperature. The spectrum of the CMB nowadays is shown in Figure 5. It will further be discussed in section 5.

2.2 Opacity

The intensity of radiation passing through a medium gets modified due to different processes in the medium, such as absorption, emission, reflection, and scattering. Opacity is a measure of how much electromagnetic radiation gets attenuated when it passes through a medium, such as the atmosphere. The amount of attenuation depends on the optical depth of the medium and the path-length through the medium. For the atmosphere of the Earth we can make an approximation it being a slab on top of the surface of the Earth. This can be seen in Figure 2. The path length of an electromagnetic ray through the atmosphere is then related by the path at zenith and the zenith angle z. The opacity of the atmosphere can be described by

$$\tau(z) = \tau_0 \cdot X(z,t) \ , \tag{2}$$

where τ_0 is the optical depth at zenith and $X(z)$ is the air mass dependent on zenith angle z which can vary in time due to temperature changes.

According to [Sweijen, 2015] the atmospheric optical depth can be considered constant during the short observation of the CMB. This simplifies equation (2), because the air mass is then only dependent on z.

$$\tau(z) = \tau_0 / \cos(z) \ . \tag{3}$$

A visual representation can be seen in Figure 2. At zenith the opacity is simple the optical depth of the atmosphere. When zenith angle z increases the path through the atmosphere becomes larger, making the value for the opacity higher.

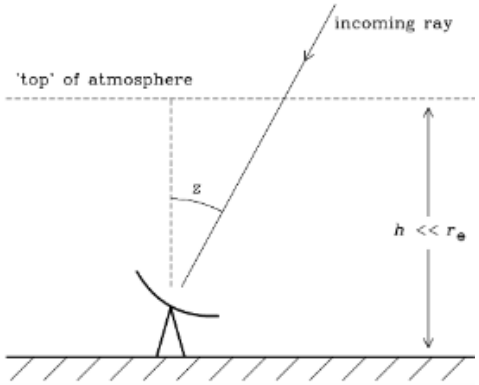

Figure 2: Opacity of the atmosphere as function of zenith angle.

2.3 Radiative Transfer

Now we know how the opacity of a medium, i.e. the atmosphere, increases as the pathlength increases, we can determine how the atmosphere will influence an observation of the sky. To understand how the intensity of radiation is changed by the atmosphere we have to look into the equation of radiative transfer. The equation of radiative transfer describes the change of intensity of an electromagnetic ray due to absorption or emission along its line of propagation. The equation of radiative transfer for a ray with intensity I_ν which is given by [Chandrasekhar, 1960] is

$$\frac{\mathrm{d}I_\nu}{\mathrm{d}s} = -\kappa_\nu I_\nu + \epsilon_\nu \ , \tag{4}$$

where κ_ν is the linear absorption coefficient independent of I_ν and ϵ_ν is the emission coefficient. This equation can be solved for some limited cases. For non thermal equilibrium cases, one can for example set the absorption $\kappa_\nu = 0$, such that the intensity of the ray only gets strengthened. This also is possible for setting the emissivity to zero, $\epsilon_\nu = 0$.

Two more interesting solutions are that of Thermodynamic Equilibrium and Local Thermodynamic Equilibrium. For thermodynamic equilibrium, thus complete equilibrium with the surroundings, the brightness distribution is simply descibed by the Planck's Function (see eq. (1)). This results in the intensity to be

$$I_\nu = B_\nu(T) = \epsilon_\nu / \kappa_\nu \ . \tag{5}$$

Equation (5) is defined as the Kirchhoff's Law. Because full thermodynamic equilibrium is not often achieved, we can consider the last solution: Local Thermodynamic Equilibrium.

In local thermodynamic equilibrium Kirchhoff's law can still be used. If we define the optical depth of the medium to be

$$\mathrm{d}\tau_\nu = -\kappa_\nu \mathrm{d}s \ , \tag{6}$$

Taking Kirchhoff's law into consideration, the equation of radiative transfer can be rewritten to the following

$$-\frac{1}{\kappa_\nu}\frac{\mathrm{d}I_\nu}{\mathrm{d}s} = I_\nu - B_\nu(T) \ . \tag{7}$$

With the substitution of the definition of the optical depth (eq. (6)), this can be solved for the intensity of the radiation at a pathlength s

$$I_\nu(s) = I_\nu(0)e^{-\tau_\nu} + \int_0^{\tau_\nu(s)} B_\nu[T(\tau)]e^{-\tau}\mathrm{d}\tau \ . \tag{8}$$

If we assume the medium to be isothermal, thus T is constant along the path, then equation (8) can be simplified to:

$$I_\nu(s) = I_\nu(0)e^{-\tau_\nu} + B_\nu(T)\left(1 - e^{-\tau_\nu}\right) \ . \tag{9}$$

2.4 Antenna Temperature

Using centimeter wavelengths, an approximation of the Planck's law can be made. Expanding the exponent in the equation and using the limit that $h\nu \ll kT$, we get that Planck's Law becomes:

$$B_\nu(T) = \frac{2\nu^2}{c^2}k_B T \quad \text{for } h\nu \ll kT \ , \tag{10}$$

where all the symbols have their usual meaning. This is known as the Rayleigh-Jeans Law [Wilson et al., 2013]. In the field of radio astronomy the limit $h\nu \ll k_B T$ can be applied often, and thus the Rayleigh-Jeans Law is used a lot in radio astronomy.

One of the important features of the Rayleigh-Jeans law is that the brightness (B_ν) and the temperature of the body (T) are proportional. This is so useful, that in radio astronomy often the brightness of an extended object is measured in its brightness temperature T. This is the temperature which would give the brightness of the source if it was put into equation (10). This results in the brightness temperature to be

$$T_b = \frac{c^2}{2k_b}\frac{1}{\nu^2}I_\nu \ . \tag{11}$$

Because of the proportionality of the brightness temperature with the brightness of the source, this can be substituted into equation (9). For an isothermal medium this equation then becomes

$$T_b(s) = T_b(0)e^{-\tau_\nu(s)} + T\left(1 - e^{-\tau_\nu(s)}\right) \ , \tag{12}$$

where T is the isothermal temperature of the medium and T_b the brightness temperature of the observed source. When observing an object through an isothermal medium, the outcome of this equation, $T_b(s)$, is the measured brightness temperature by the antenna. This is thus also known as the *antenna temperature*. Important is to remember the antenna temperature is thus not the physical temperature, but rather an value for the measured brightness of the source.

3 Noise

3.1 System Noise

The output of a measurement system is not only that of the observed source. A measurement system, such as a telescope, adds its own signal to the measured signal. This noise is described as the receiver noise, which can also be expressed as an equivalent noise temperature. This results in the total output of a measurement system to be the measured signal plus its own receiver temperature. This is called the system temperature

$$T_{sys} = T_a + T_{rcv} \ , \tag{13}$$

where T_a is the antenna temperature and T_{rcv} is the receiver temperature. Not only the system itself adds noise, but the antenna temperature is not that of the observed source alone. A lot of other signals can contribute to the antenna temperature, such as ground radiation or scattered radiation from buildings.

The added receiver noise has to be determined before useful information can be gained from the data. This can be done by performing calibration on the measurement system. This calibration is described in section 3.3.

Along with the receiver noise, the precision of a measurement also depends on the measurement uncertainties and the systematic uncertainties. These equations are well written out and derived by Willeke [Mulder, 2015].

3.2 Allan Variance

The Allan Variance is a measure of stability of clocks or amplifiers. It is named after D.W. Allan and is mathematically shown as $\sigma_y^2(\tau)$ [Allan, 1966]. The Allan Variance is used to estimate the stability of a system. The instability of a system comes from frequency instability and flicker noise of the system. To calculate the Allan Variance a data set is divided in bins based on some averaging time. At first the average of the first bin is calculated, this is compared with all following bins and the differences are summed. This sum is divided by the total number of bins, giving the Allan Variance as a function of averaged time. A mathematical definition is

$$\sigma_y^2(\tau) = \frac{1}{2(M-1)} \sum_{i=1}^{M-1} (y_{i+1} - y_i)^2 \ , \tag{14}$$

where y_i is the average of a set of values in the ith bin over the measurement interval $(t, t+\tau)$. The Allan Variance gives a good representation over which time interval a measurement system can be trusted. The maximum time of a measurement should be that of when the Allan Variance is minimum. The Allan Variance of the telescope is calculated by [Zandvliet, 2015], his work and scripts are used in this project.

3.3 Calibrating a Measurement System

Calibration of a measurement system is important, because without this calibration, the data gained from an observation can not be interpreted. A good calibration method is the y-factor method. This method uses two black body radiations as loads with different known temperatures, a hot load and a cold load. The output of the measurement system is related to the input and the *gain* of the system. This gain of the system is the amplifier gain, which is the amount of times the signal gets boosted by the back-end of the system. The output can be related to the input with

$$\begin{aligned} z_{\text{cold}} &= (T_{\text{cold}} + T_{\text{rcv}})G \\ z_{\text{hot}} &= (T_{\text{hot}} + T_{\text{rcv}})G \end{aligned} \tag{15}$$

where z is the output power in terms of the bandwidth and Boltzmann constant. Defining the y-factor to be $y = z_{\text{hot}}/z_{\text{cold}}$, the receiver temperature can be determined with [Yfa, 2001]

$$T_{\text{rcv}} = \frac{T_{\text{hot}} - T_{\text{cold}} \cdot y}{y - 1} \tag{16}$$

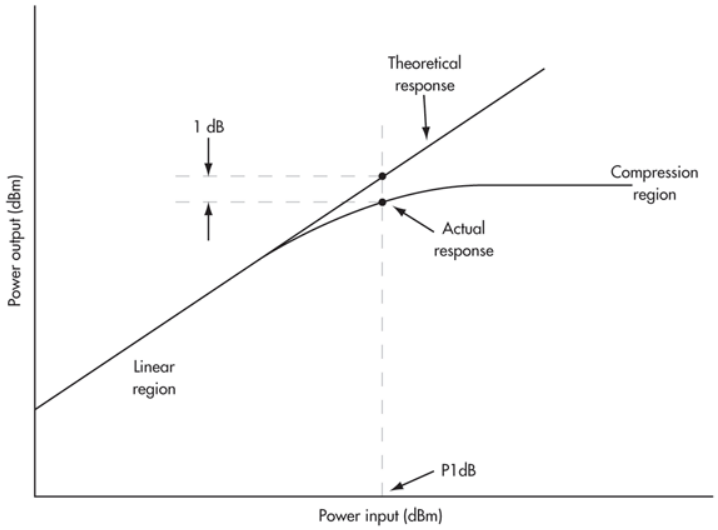

Figure 3: Linear response of a system. The point where the gain decreases 1 dB is called the 1-dB compression point. [Frenzel, 2013]

This calibration method assumes that the response of the system is linear with the incoming signal. This can be seen in Figure 3, where an visualization is made for the response of a system. Observations with a system following this curve should be made in the linear regime far below the 1 dB compression point in order to get good results.

4 The Kapteyn Radio Telescope Project

4.1 Introduction

The Kapteyn Radio Telescope (KRT) is a radio telescope made in 2015 by four astronomy bachelor students for their bachelor project. The goal of that project was to make a telescope which can measure the temperature of the CMB. The telescope is used for the course Introduction to Radio Astronomy given to third years astronomy bachelor students on the University of Groningen. The practical assignment with the telescope gives a great view of all the subjects in the field of radio astronomy and helps understanding concepts used in the course. The four students each researched and made a different part of the telescope. Their work was put together to make the telescope.

Bram Lap focused in his thesis on the design and building of a horn antenna for the telescope. Maik Zandvliet researched what the best back-end was for the telescope and made the construction of it. Frits Sweijen developed the control of the telescope. With the telescope ready, Willeke Mulder did the calibration of the telescope.

4.2 Telescope Components

Horn Antenna

The KRT is a horn antenna telescope. The horn antenna was made and designed by Bram Lap [Lap, 2015]. In his thesis he researched different horn antenna types which would fit the best for an observation of the CMB at 11 GHz. Eventually the Picket-Potter horn was the best for the requirements. This horn design came out to have to best beam pattern for an sky observation of the CMB. The side lobes are low enough such that they should not interfere with the observation. The full width half maximum of the primary beam of the beam pattern was set to an maximum value of 15°. After building the horn, testing the beam pattern with a radiation emitting source showed that the horn met its requirements to be put on the telescope.

The horn antenna consists of two parts: the copper horn itself, and an aluminum waveguide (Fig 4a). These parts are put together, such that there is a transition from the horn to the waveguide. Due to the nature of the Picket Potter horn, the transition between these two parts determine the parameters of the telescope. With multiple simulations the best parameters were determined for the horn. After building the horn and the waveguide the horn was tested for its beam pattern (more on the beam pattern in section 9.2). With the outcome of these tests the best orientation of the horn could be determined.

Front-End

While the horn antenna couples the observed radiation to a signal, it can not directly be measured. The Front-End of a telescope is normally the horn and a series of components which directly converts the signal such that it can be processed with a computer. On the KRT there is a series of two amplifiers and a bandpass filter. The outcoming signal gets measured with a power meter [Zandvliet, 2015]. The power meter displays the wide-band electrical power of the measured signal, which can be written down, or saved on a computer.

(a) The copper Picket Potter horn with its aluminum waveguide [Lap, 2015].

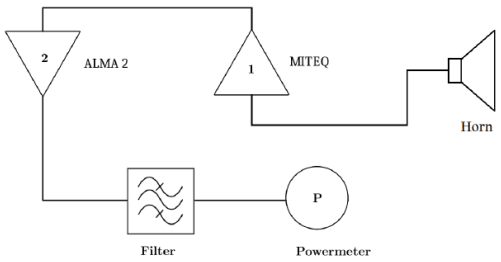

(b) *front-end:* Horn and Amplifiers (MITEQ, ALMA2). *Back-end:* Filter and Power Meter [Zandvliet, 2015].

Figure 4: The KRT horn antenna and its components.

An amplifier is a device that increases the power of an incoming signal. It gets powered by a power supply and amplifies the incoming signal to a higher amplitude. This amplification is characterized as the *gain* of the amplifier, which is the ratio of the output to the input of the amplifier. As an amplifier makes the signal easier to measure, it also contributes a lot to the noise of the total system. A good amplifier has low internal noise, is linear and has a stable gain. It should also have a flat response over a certain range of frequencies, it should not have the properties of a filter.

A filter is a device which filters out unwanted signal. For the design of the telescope the observing frequency was chosen to be 11 GHz, with a bandpass of 1 GHz. To meet these requirements a filter was used which only lets signal through in the range 10.45 GHz $< \nu <$ 11.50 GHz, making the bandpass due to availability of equipment to be 1.05 GHz.

Another commonly used device in radio astronomy is the mixer. This device shifts the incoming sky signal to a lower frequency. This is done by combining the incoming signal with a signal from a local oscillator of a very well defined frequency. The outcoming signal has its frequency lowered. This signal is easier to use, because only one sort of filter is required if all the incoming signals are down converted to a frequency of that filter. Also amplifying signals of very high frequency is simply not possible.

Frame

For an observation of the CMB multiple measurements of the sky have to be made of a different altitude. To make these measurements as precise as possible the full telescope setup, horn antenna and components of the back-end is mounted with a stepper motor on an aluminum frame. This frame consists of 20x20 mm aluminum bars which are put together with plastic connectors[2]. In this way the horn antenna can be rotated in zenith angle controlled by a computer. This gives the best precision when taking a measurement of the sky.

[2]http://www.voliereonderdelen.nl/shop2009/index.php?cPath=22 accessed: June 2017

To make an observation as easily as possible the hot and cold load of the system are mounted in and under the frame, such that the telescope can look at the loads. This makes a full observation of the sky simply one press on a button. The telescope moves to the hot and cold load for the calibration and continues to do its observation of the sky.

Computer Control

The telescope is controlled with a self made laptop controlled system by Frits Sweijen. This system is based around a Raspberry Pi[3] with its own local network [Sweijen, 2015]. For a fully functioning telescope it was required to have all the parts of the telescope controllable by the Raspberry Pi. This includes communication with the stepper motor and reading out of the power meter and temperature sensor of the hot load. Additionally, some power supplies were needed to power the stepper motor and the back-end of the telescope. To use the telescope, a laptop can be connected to the local network, giving full access to the Raspberry Pi. Frits wrote a telescope server program in which an user can control the stepper motor and start their observation. This is all documented in [Sweijen, 2015] and [Lap et al., 2015].

4.3 Calibration of the Telescope

Calibration of the measurement system has to be done for every single observation. This is to ensure the calibration of the system is the closest to the observation itself. This is done because of the drift of the response of the system, such that the response is known at the time of the observation. Calibration is done by using the y-factor method described in 3.3. The hot load is radiation-absorbing material (RAM) mounted on the frame itself which is the same temperature as the environment. Its temperature is measured with temperature sensors. The cold load is that same absorbing material in a box with liquid nitrogen (77 K). This RAM is a material specifically designed to absorb any radio frequency radiation from any direction as efficiently as possible, it will then emit as a black body. The most effective type of RAM is an array of pyramid shaped pieces. Absorbers used in this project are coming from ASTRON, where it is used in an anechoic chamber. All the incoming radiation on the RAM is absorbed in the observed frequency band, so the only radiation coming off it is that of a blackbody. The power measured of the load is thus the brightness of the Planck's function given the temperature of the material. Having the hot load on the frame of the telescope gives that its temperature is the same as that of the environment the telescope is in. The cold load is the absorber immersed in liquid nitrogen, thus is the black-body curve with a temperature of that of boiling liquid nitrogen.

These loads are placed in such a way that the horn can rotate to the loads. In this way an observation can include the calibration. In the original frame the cold load could be seen by the horn via a mirror.

[3]Raspberry Pi 1.2 Model B+

4.4 Properties of the Kapteyn Radio Telescope

The KRT will undergo some changes in this thesis. A reconstruction of the frame (section 6) and a change in front-end components (section 7) as a upgrade will (hopefully) improve the telescope's accuracy. In Table 1 a few properties are listed of the original version of the KRT. The sky observation time is a typical time for a full CMB observation.

Property	Value
Observing Frequency	10.45 GHz - 11.5 GHz
Primary Beam Full Width Half Maximum	12.92°
Gain	60 dB
Receiver Temperature	180 - 200 K
Sky observation time	80 s

Table 1: Values for the original KRT. Sources: [Mulder, 2015], [Lap, 2015]

5 Measuring the Cosmic Microwave Background

The Cosmic Microwave Background radiation follows the Planck's function of a black-body. This curve is shown in Figure 5, where we can also see the observing band of the Kapteyn Radio Telescope. This shows that the observing band is in a really low intensity range of the CMB. The CMB can therefore better be measured in a higher frequency band.

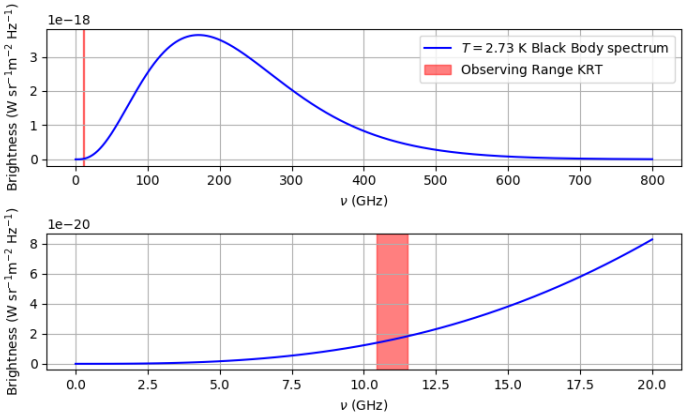

Figure 5: Black-body spectrum of the Cosmic Microwave Background Radiation. In both plots the observing range of the KRT is shown. Bottom plot: expanded on observation band.

The problem with observing in a higher frequency band is the opacity of the atmosphere. At higher frequencies the opacity gets a lot higher due to water vapor and water lines (see Fig 6). With this limit and the availability of equipment it was determined to have the KRT observing at 11 GHz.

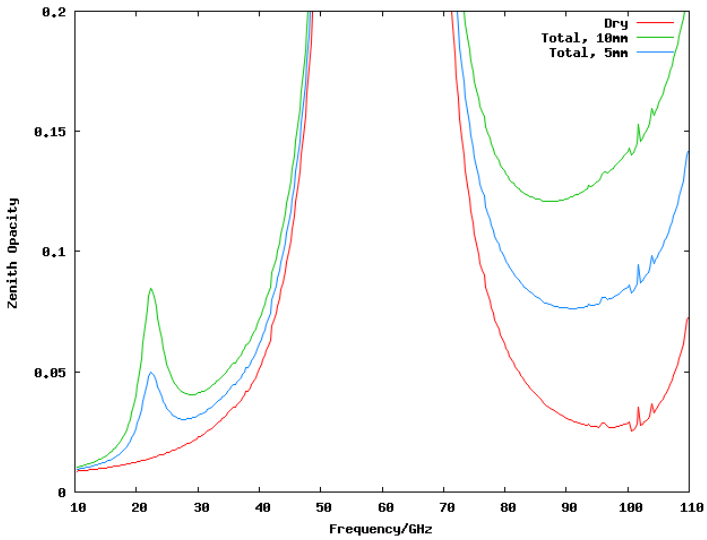

Figure 6: Atmospheric opacities at zenith for a dry atmosphere, with 5mm precipitable water vapor (pwv), and with 10mm pwv. Values calculated by ATM for the elevation of the Green Bank site [Opa, 2017].

We will measure the CMB through the atmosphere with the telescope, so the equation for antenna temperature can be applied to this observation. Taking the CMB as a source and the atmosphere as the medium the radiation is traveling through (assuming isothermal), the antenna temperature of the telescope is then given by (derived in section 2.4)

$$T_a = T_{\text{cmb}} e^{-\tau_0 \sec(z)} + T_{\text{atm}} \left(1 - e^{-\tau_0 \sec(z)}\right) \ . \tag{17}$$

For a single measurement at a zenith angle z, there are still too many unknowns. Equation 17 can only be solved when multiple measurements are taken at different angles z. This is a full sky observation, where the telescope takes multiple measurements of different zenith angle z. This gives a curve of the measured sky power, on which equation 17 can be fitted to solve for the unknowns.

A measurement starts with the calibration of the telescope. The horn first points at the cold load, then at the hot load. Because the absorber is optically thick ($\tau \gg 1$) and the absorbers are in thermal equilibrium with their surroundings, equation (17) gives that the antenna temperature is only that of the temperature of the load ($T_a = T_{\text{atm}}$ or $T_a = T_{\text{cold}}$). These powers are saved and the receiver temperature can be calculated with equation (16). The horn will scan through zenith and start its sky observation.

The power displayed on the power meter is shown in dBm, which is the power in dB with respect to 1 mW. This relation is converted to real values with

$$P[\text{mW}] = 1\text{mW} \cdot 10^{(P[\text{dBm}]/10)} \ . \tag{18}$$

This output power can be related to the system temperature with

$$P_{\text{out}}[\text{W}] = T_{\text{sys}} \ k_b \ \Delta v \ G \ , \tag{19}$$

where Δv is the bandwidth of the telescope and G is the amplifier gain of the back-end. The other symbols have their usual meaning. To get the output power of the telescope to a system temperature, the amplifier gain has to be calculated. This can be done using data of the y-factor calibration with the following equation:

$$G = \frac{P_{\text{hot}} - P_{\text{cold}}}{k_b \Delta v (T_{\text{hot}} - T_{\text{cold}})} \tag{20}$$

With the gain known the output of the observation can be converted to system temperature. Then applying a fit with equation (17) on the data returns the values for the temperature of the CMB and the opacity of the atmosphere.

6 Reconstruction

6.1 Goal

While the Kapteyn Radio Telescope project as a whole was a success, there were still a few problems remaining. In this thesis we addressed these problems and tried to think of a solution for them.

6.2 The Problems

During the Introduction to Radio Astronomy course we also did the practical assignment with the KRT. It was already made clear beforehand that the telescope had some issues with its observation. Eventually the outcome of the temperature of the CMB was indeed way off, and even negative with a temperature of -6 K. The reason for this offset was not completely known at the moment, while there were some guesses what it could be.

Looking at the Thesis of Willeke Mulder she points out that the cold load box is too far from the horn, thus not filling the entire primary beam. This results in extra signal from outside the box. She advised a bigger cold load, or closer to the horn. This means that a reconstruction of the frame has to be done.

Another improvement to the system could be the reduction of the receiver temperature. This was not discussed by any of the students who made the telescope, but was talked about during the start of this project. Lowering the receiver noise should increase the signal to noise ratio. If the integration time stays the same, a better signal to noise ratio gives better accuracy. This can also be seen the other way around, less integration time is needed to give the same result.
To improve the telescope we decided to do the following upgrades:

1. Rework the frame of the telescope, such that the calibration can be done better.
2. Lower the receiver noise temperature, such that the signal to noise ratio is higher.
3. Make the sky observation faster, such that the observation is within the time that the calibration is reliable.
4. Make the system easier to move and use, such that it can be quickly set up when the weather gets favorable.

6.3 Testing and Building

One of the primary goals with the reconstruction of the frame was that the hot and cold load should definitely fill the entire primary beam of the horn. Because of the beam pattern of the telescope, having the hot and cold load in the far field would require too big loads. Thus having the loads as close as possible should have the same effect, because then there is only a load in the direction the horn is facing. This resulted in the decision to put the cold load directly u the hornnder, such that when the horn is facing downwards it only sees the cold load.

Frame

With the cold load moved directly under the horn, there was suddenly a lot of space for the hot load. This means that if the hot load is placed efficiently, the horn can make a more extensive sky scan. The horn can start 'before' the zenith, and go through the zenith to the horizon. At the start of the project I first had to investigate how everything works precisely on the telescope before taking it apart. The computer control system could easily be taken apart from the telescope, leaving only the frame with the horn and back-end on it. The initial idea was to have the cold load directly under the horn and the hot load to be next to it at a slight angle. This turned out to be mechanically difficult and would not gain an improved observation in comparison with the hot load 90° with respect to the cold load (see Fig 7).

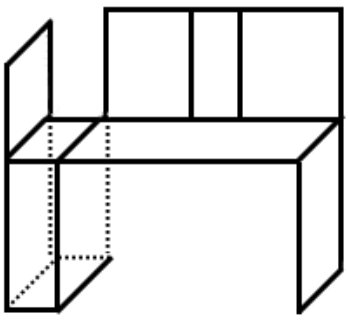

(a) Drawing of the new frame 3D.

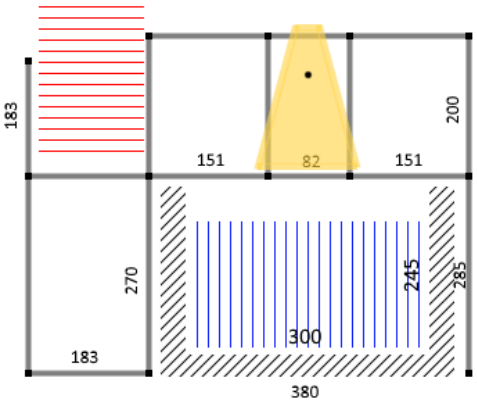

(b) Size view of the frame. *Striped areas:* hot and cold load. *Yellow:* The copper horn. The connectors are indicated with the black squares. The numbers are lengths of the aluminum bars and EPS box dimensions.

Figure 7: Drawings of new frame.

When the horn is facing down, as in Figure 7b, then the cold load is as close as possibly can. The absorber needs to be fully under the liquid nitrogen to be in full thermal equilibrium. Because the liquid nitrogen evaporates rather quickly, a layer of minimum 1 cm needs to be above the absorber. Also a few centimeters are required for the horn to freely rotate. This comes down to that the cold and hot load are on approximately 4-5 cm distance from the horn when the horn is directly facing them. With this frame, the horn can point right in the middle of the hot and the cold load.

Cold Load Box

When the telescope was being built the students had trouble finding a polystyrene box that was suitable as a cold load box. The box should be big and high enough such that the absorber can fit in the box. They did not find any box that had the dimensions of the absorber, so they had to cut off the top of the absorber so it could fit in (see Figure 8a). This should in theory still work as a full absorber. Due to the small box and the distance from the horn to the cold load box the primary beam of the telescope could see partially outside the box. To tackle this problem we thus need a new cold load box with the right dimensions and thickness. The best material of the box needs to be strong enough such that it can be moved with 20 liters of liquid nitrogen. Also the material needs to isolate against the temperature differences of the liquid nitrogen and the environment.

(a) Old cold load. **(b)** New cold load.

Figure 8: Cold load absorbers.

The material that was used as the original cold load is called Expanded Polystyrene (EPS) and suited well for these requirements. It was required that the new cold load box would be a perfect fit for the frame and the absorber inside it. This was to make sure that the beam of the telescope is fully facing the cold load. An EPS box was found and bought online[4], this box was made for dry ice transport and the dimensions fitted perfectly. The inner dimensions are 300x300x300 mm, making the base perfect for the absorber. A few centimeters were cut off the top of the box with a hot wire to fit under the frame. To shield from stray radiation coming into the cold load, the inside of the box is plated with metal plates. This is needed because the polystyrene box is completely transparent for electromagnetic radiation of 11 GHz. The metal pates are conductive, so any radio waves get reflected of them. On top of keeping stray radiation out, any radiation that is in the box also gets reflected. This radiation gets reflected right back into the absorber, making the probability of absorbing higher. It makes sure that the side lobes of the horn are also terminated in the cold load.

The final new cold load box can be seen in Figure 8b. Not only is the absorber area bigger, but the box is better shielding against stray radiation. The reflecting material is now inside the box, touching the liquid nitrogen. With the old box setup it first had to pass through the warm polystyrene and then get reflected by the aluminum foil. This foil was also not perfect, because of the flexibility of the material. Overall the new cold load box should give more accurate calibration.

Stepper Motor

The time it takes for a CMB observation depends mostly on the stepsize in zenith angle of the observation, but also the speed of the stepper motor contributes to the time. Moving from the cold load to the hot load, and then to the start of the observation is already a third of the observation time (approximately 15 seconds.). With an Allan Variance of the old system of $\sim$10 seconds [Zandvliet, 2015] this is already too long. Increasing the stepper motor speed is then obviously important.

[4] http://www.droogijs-amsterdam.nl/box-25.html

Increasing the stepper motor speed required us to replace the stepper motor as a whole, including its controller. The original stepper motor was a high ohmic motor controlled by applying a voltage. It is replaced with a low ohmic motor which is controlled by the current. This required a new controller which could apply this current. The stepper motor controlled was provided to us and was integrated into the system. The controller was added to the local network, such that it could be controlled with the telescope server. For a even faster operation a stronger controller board could be implemented in to the system. This could be used in the future with an even better stepper motor.

Complete Construction

With the frame complete and the cold load box complete, this is the picture of the telescope now (Fig 9). The horn gets mounted on the round disk and can freely rotate to the hot and cold load. As the reader can see, the frame is now compact, so the horn is close to the loads. Also a second box has been made for the measurement equipment and power supplies. This makes the telescope easier to move without having connect everything again at every setup for observation. The telescope can now be moved on a single trolley. The equipment is shown in Figure 10

, 2017

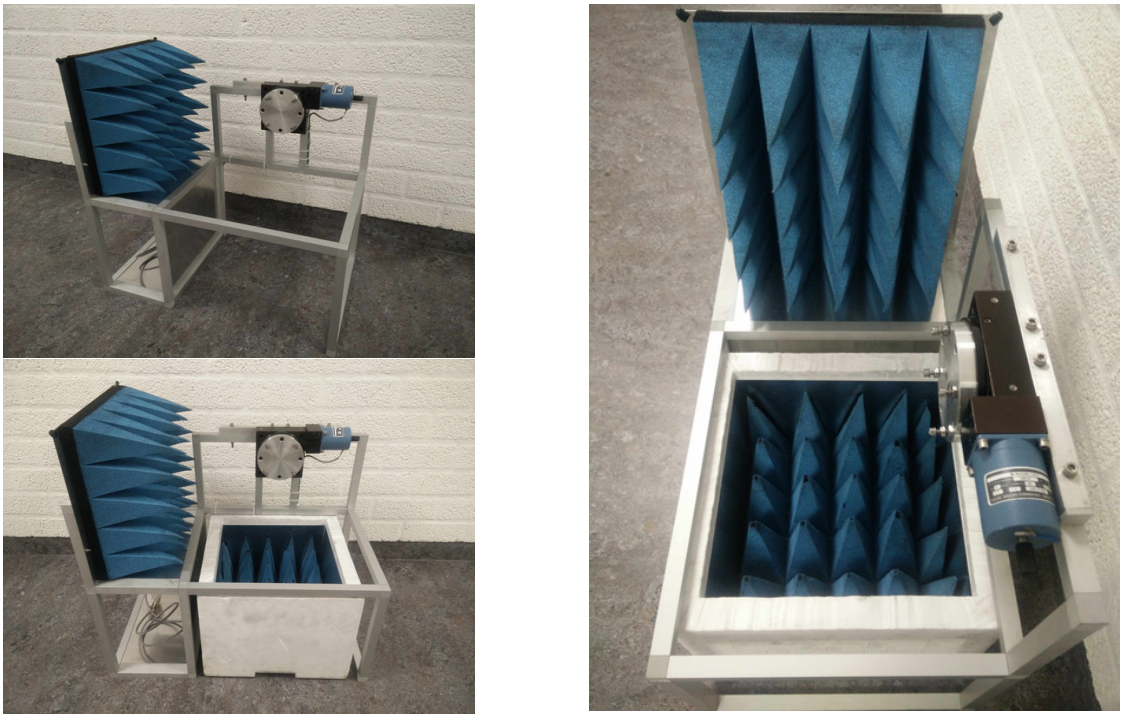

Figure 9: Complete frame. The hot load is the absorber mounted on the frame, which is the same temperature as the environment. The cold load is the white polystyrene box with the absorber in it. For an observation liquid nitrogen is inserted. The round plate is a rotator, which is part of the stepper motor on which the horn is mounted.

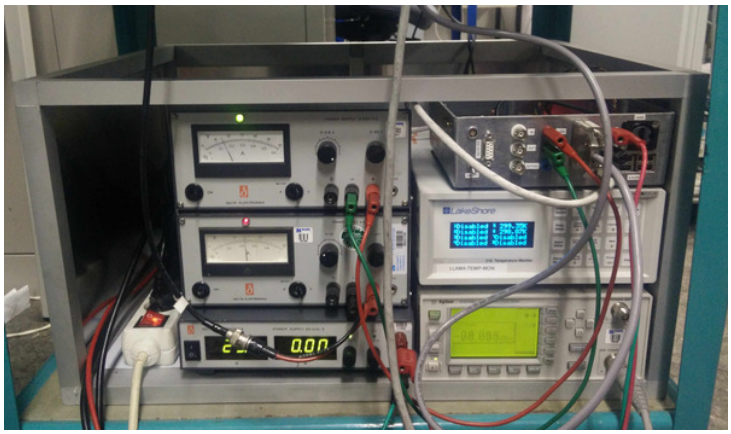

Figure 10: Measurement equipment and power supplies for the KRT. A total of 6 devices are used. The three devices on the left are the power supplies. The three devices on the right are from top to bottom: Stepper controller, temperature meter, power meter.

7 Low-Noise Block Downconverter

7.1 General Use

The low-noise block downconverter (LNB) is a small receiver device which can be mounted on a satellite dish for receiving television signals. A typical single feed LNB (see Fig 11a) gets mounted at the focus of the satellite dish, such that all signals transmitted by the satellites gets reflected into the LNB. The signal is picked up by a small feedhorn and gets into the waveguide. In the waveguide, one or multiple small waveguide probes pick up the signal. In Figure 11b an LNB is cut in half, showing the feedhorn and the waveguide. After the signal is received by the antenna, it gets processed by the components inside the LNB (see section 7.2).

There are a few properties of LNBs which are very interesting for this project. LNBs are made to receive and process incoming signal for television. For the best quality television the noise temperature of the LNB should be as low as possible. This can be seen in the way how companies advertise their LNBs. Every LNB is sold with a number for its noise. For example, the LNB shown in Figure 11 is advertised to have a noise figure of 0.7 dB as a maximum. This is equivalent to an receiver temperature of approximately 50 Kelvin. Another property which makes the choice of an LNB interesting is the fact that the frequency range of the satellites in Europe is the same as the frequency range our Picket Potter horn is optimized for. The horn is optimized for the frequency 11 GHz, the ASTRA[5] satellites use two different bands for sending television signal, one band is in the frequency range 10.7 GHz to 11.7 GHz and the other band from 11.7 to 12.75 GHz. The bandwidth is 1 GHz, the same as the back-end of the KRT [Zandvliet, 2015].

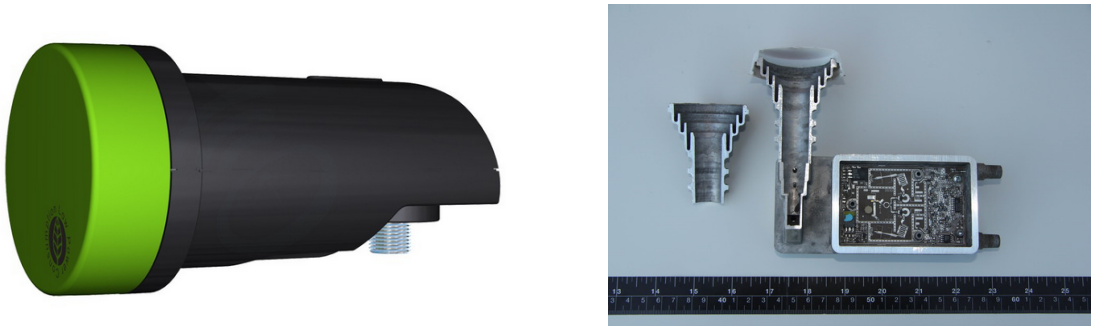

(a) Typical Single LNB sold in stores.

(b) LNB cut in half.

Figure 11: Low Noise Blocks

7.2 Components in the Low Noise Block

If the radiation received is picked up by the probes, the signal comes into the LNB. In the LNB there is an PCB with components on it to process the incoming signal. These components include a series of amplifiers, mixers and local oscillators. The received radio frequency (RF) signal is amplified to a higher amplitude and mixed down to a lower intermediate frequency (IF).

[5]Satellites for television in Europe.

For the KRT project we are only interested in the power output of the system. So the frequency shift is a nice addon, but it is not needed. The components in the LNB are a two stage radio frequency low-noise amplifier, frequency mixer, local oscillator and intermediate frequency amplifier. A schematic of these components is shown in Figure 15. Comparing this with the schematic of the KRT (see Fig 4b) we can see there is a lot more components inside.

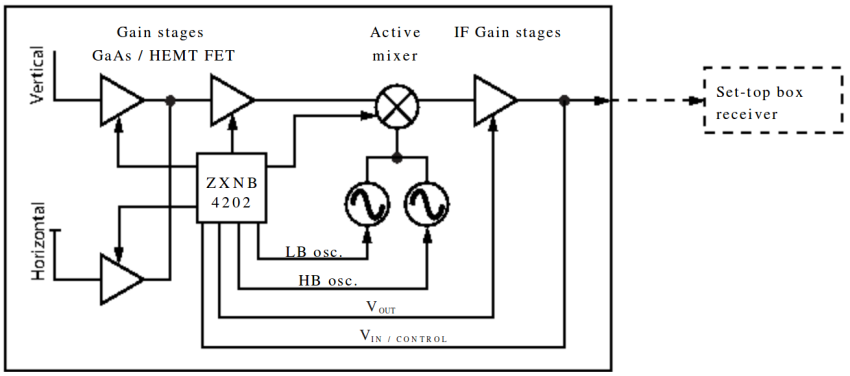

Figure 12: Sinle LNB system diagram [lnb, 2010]

An LNB can receive signal of two linear polarizations, this is done so that twice the signal can be received from the satellites. This incoming signal gets first amplified by the RF amplifiers and passed through the mixers. These mixers are tunable so that the incoming signal always gets shifted to the same intermediate frequency. The signal gets amplified again by an IF amplifier before leaving the LNB through a coax cable. Tuning of the polarizations and the observing band can be done by applying different current and voltages to the LNB through the coax cable. The observing polarization and band which are used per applied voltage and current is shown in Table 2. Combining the different polarizations and the tone on the current, the universal LNB can receive signals in four sub-bands. Control of the mixers and amplifiers is done by the main control chip in the LNB. Information about this chip was unfortunate classified.

Voltage	Tone	Polarization	Frequency Band	LO Frequency	IF Band
13 V	0 kHz	Vertical	10.70-11.70 GHz	9.75 GHz	950-1950 MHz
18 V	0 kHz	Horizontal	10.70-11.70 GHz	9.75 GHz	950-1950 MHz
13 V	22 kHz	Vertical	11.70-12.75 GHz	10.60 GHz	1100-2150 MHz
18 V	22 kHz	Horizontal	11.70-12.75 GHz	10.60 GHz	1100-2150 MHz

Table 2: Observing bands and polarizations of a universal LNB.

The power control is normally done by a television box, but in our case we only have a power supply. Because there is only one connector on the LNB, the power input and the signal output have to be combined. This is done with a bias-tee (see Fig 13), the name comes from the typical shape of an T. The bias-tee is an easy way for setting a DC power bias on an electronic device without disturbing the outcoming signal. The combined bias and signal (left side Figure 13) goes to the LNB, the right side goes to the power meter.

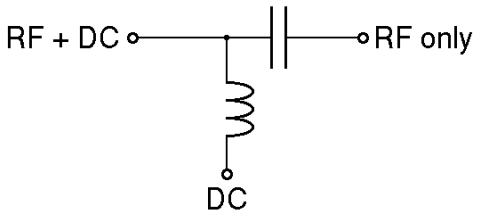

Figure 13: Schematic of internals of a Bias T.

7.3 Low Noise Block on the Telescope

We can say that the LNB consists of roughly three parts: the feedhorn, the waveguide and the amplifiers/mixer board. Because the LNB has a expected lower receiver temperature, we want to integrate the LNB into the telescope. For this we choose which components we want to preserve of the current telescope. Because of the extensive beam pattern of the LNB, we want to keep the horn of the telescope. This horn is already optimized with the best beam pattern and for the right frequency. So the LNB will replace the waveguide of the picket potter horn.

For the integration there needs to be a smooth transition between the waveguide and the LNB. In the design of Bram Lap the waveguide has its own transition onto it, because it is cut from one piece of aluminum. In Figure 14a the transition between the horn and waveguide is shown. To get the same transition between the LBN and the horn an aluminum flauge has to be made.

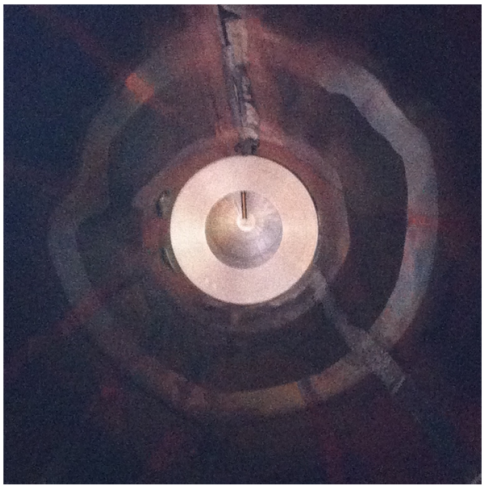

(a) Original transition from the horn to the waveguide.

(b) New transition to the LNB (zoomed), clearly the two polarization antennas can be seen. Included is a big pin which serves as filter.

Figure 14: Transition from copper horn antenna to aluminum waveguide.

Mechanical Work

We determined the best method to attach the LNB to the horn is making a piece of aluminum which looks like the waveguide made by Bram Lap [Lap, 2015], but have the LNB replace the waveguide part, thus only leaving the transition from the horn to the waveguide. The transition should be made such that the LNB can be slided in into the new piece of aluminum. In Figure 15 the drawing of this flauge is shown. The top side is attached to the horn and on the bottom side the waveguide of the LNB can be slided in. This requires that the feedhorn of the LNB has to be cut off. In Figure 16a the two LNBs are shown with the feedhorn cut off. Also the outside of the waveguide is cut to precisely match the inner dimensions of the aluminum flauge. The outer radius of the LNBs match the inner radius of the flauge of 20 mm. Two flauges were made for two different LNBs, so that both LNBs could be tested when mounted on the horn.

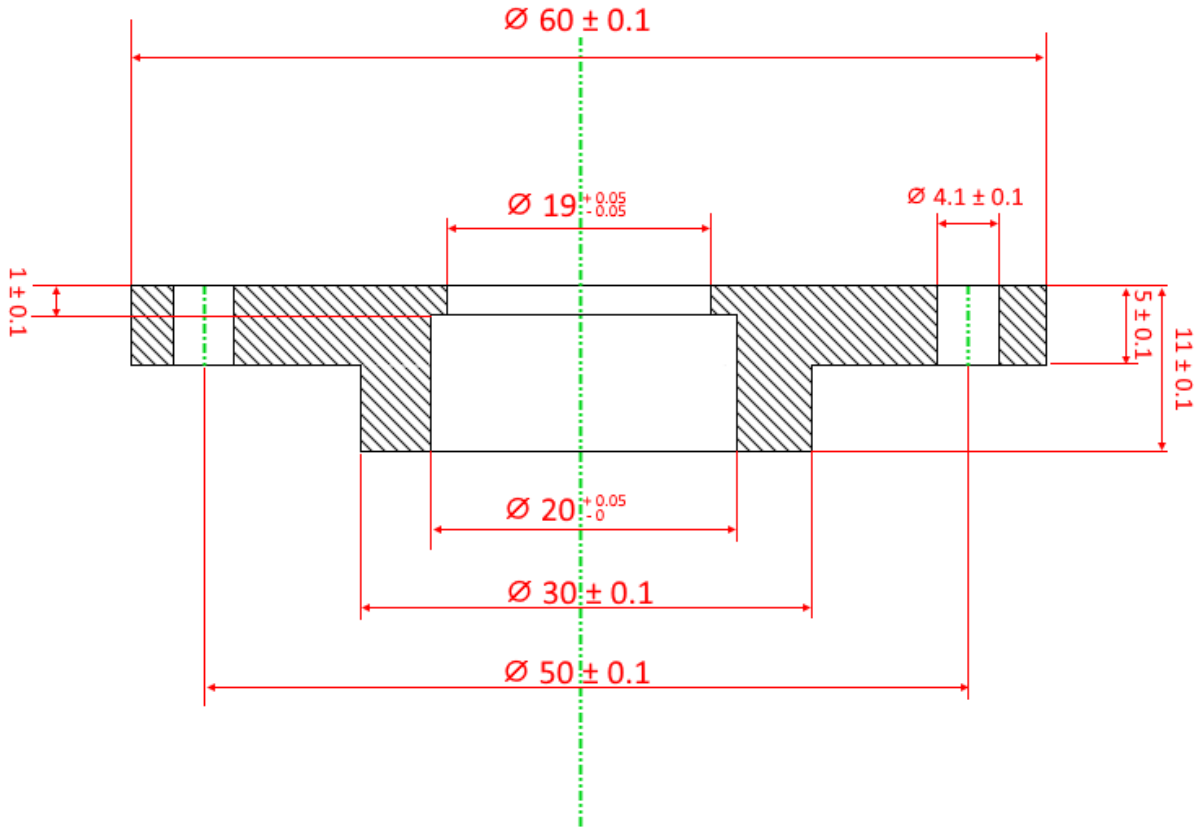

Figure 15: Drawing of the aluminum flauge to connect the LNB to the horn antenna.

In Figure 16b the new transition is shown, this can be compared with the old transition in the same picture. Clearly can be seen that the part that fits to the horn is the same and the waveguide can now be replaced with an LNB. In Figure 17 an LNB is put into the aluminum flench, showing that is fits perfectly. The only thing left is securing the LNB into the aluminum flench, by glueing it with a conductive epoxy glue.

The LNB is now secured on the horn. A bias t is connected to the horn via SMA cable and a SMA to BNC connector. The power meter of the old system is used to read out the signal. The complete system is shown in Figure 18.

(a) LNBs cut with lathe. Feedhorn is cut off and the outer radius is cut to 20 mm.

(b) *left:* New flauge. *right:* Old waveguide

Figure 16: New parts for the horn.

Figure 17: An LNB in the flauge compared with the old waveguide.

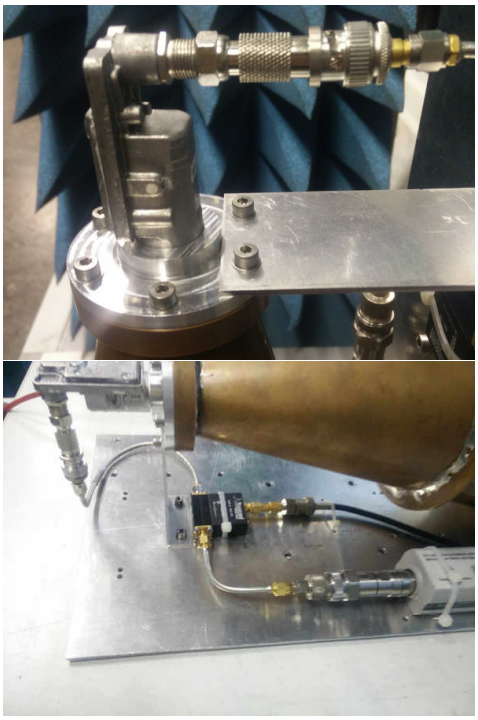

Figure 18: LNB mounted on the horn with its components.

8 Testing and Calibration

During the project, a total of three LNBs were obtained to test. We needed multiple LNBs to test them against each other, so get the best LNB on the telescope. The LNBs were tested on their stability of the output and their system temperature. The LNB with the best results was put onto the telescope. The LNBs we got are listed in table 3 along with their advertised properties when they were available. The Inverto and Amiko LNB were both modern LNBs. We also obtained an older LNB, the Phillips, because we thought it would be a more discrete system and thus easier to modify. The noise figure in table 3 is related to the noise temperature of the system. The values 0.1 and 0.7 dB are related to noise temperates of 10 and 50 Kelvin respectively.

Name	Type	Noise Figure	Gain
Inverto LNB ECO Single 41mm LNB	Universal LNB	0.7 dB	50-60 dB
Amiko Single LNB Premium Slim L-103	Universal LNB	0.1 dB	-
Universal Single-LNB PHILIPS SC819TB	Universal LNB	-	-

Table 3: The three obtained LNBs with their advertised specifications (where available).

The first step we took was looking at the internals of the LNBs. They were taken apart and the PCB found inside was examined with a microscope. Because the first LNB we got was the Amiko LNB, the following information is about that LNB. A picture of the PCB and its components on it is shown in Figure 19. Its schematic was already shown in Figure 12. Next to the purple diamonds are the probes going into the waveguide of the LNB. Further information about the control chip was not available. The documentation of the control chip was classified, and only showed the schematic of a typical system using that control chip [lnb, 2010].

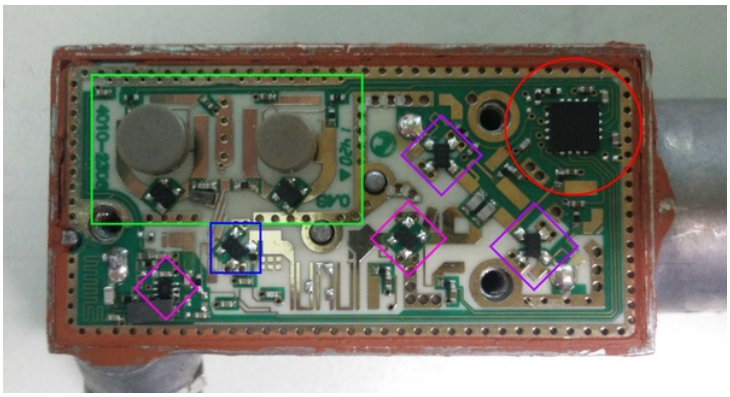

Figure 19: PCB of Amiko LNB. *Red circle:* control chip. *Green square:* local oscillators. *Diamonds:* amplifiers. *Blue square:* mixer.

Taking apart the Inverto LNB showed the same layout on the PCB, only with different control chips. This board also had a crystal oscillator instead of a variable-frequency oscillator. The Phillips LNB was a lot different than the other two LNBs, the components were more discrete. No documentation was found of the components inside, probably due to the age of this LNB.

8.1 LNB tests

With these three LNBs on the table, we needed to know which was would have the best stability and receiver temperature so it can be put on the telescope. First tests were done by holding the LNB in hand, thus yielding unstable results. The two tests we did were the hot and cold load tests and a stability test. This was done by pointing the horn at a bucket with liquid nitrogen as a cold load and our own absorber as a hot load. The first results were rather weird, because sometimes the receiver temperature would be negative. This is physically not possible, so we thought of an explanation for this.

At first, we thought there was a variable gain amplifier in the LNBs. Pointing the LNBs at the hot load and at the cold load gave similar power outputs of the LNBs. This could be explained by the amplifiers boosting the signal more when looking at a much colder cold load. A lot of time went into figuring out if this was the case and how we could stop it from changing. For this exact reason the third Phillips LNB was tried, because the hypothesis was that such an old LNB would not have such an 'advanced' system.

It turned out, that after the new cold load box was finished, that the absorber in the bucket which we used as cold load was completely transparent for our frequency of 11 GHz. This resulted in reflections of radiation from the environment in the bucket. With the new cold load box, which is an excellent absorber at 11 GHz, the receiver temperature tests went a lot better. First tests were done with a sloppy connector cable, so receiver temperatures were deviating a lot. The results of the different LNBs are listed in table 4. These tests were done on the same day in an environment where the temperature did not fluctuate more than 1 degree during the tests.

LNB	Receiver Temperature (K)
Amiko	148.5
Amiko	137.1
Amiko	130.3
Inverto	107.7
Inverto	115.3
Inverto	114.5
Phillips	281.0
Phillips	205.1
Phillips	343.6

Table 4: Hot Cold load test of the LNBs

From these first tests it was clear that the Amiko and Inverto LNBs perform better than the Phillips LNB. We continued testing with these and stopped testing the Phillips LNB. The results of the tests were pretty widespread. A lot of fluctuations in the receiver temperature, as well as the power output was seen. This fluctuations were probably due to the bad hand made connector between the LNB and the SMA cables. With a better connector the power output was more stable, and hot cold tests showed more of the same temperatures. After a lot of testing with putting the LNBs in the liquid nitrogen, eventually the Inverto LNB had the best results.

Using the new connector a few more tests were done, yielding the receiver temperatures listed in Table 5. These tests showed a more stable output of the receiver temperature. The only thing left that could influence the unstable results was the extended beam pattern of the LNB. When mounted on a satellite dish it needs to have this extended beam. Using it on the smaller cold load gives that stray radiation from outside the loads could be measured. Securing the LNBs on the copper Picket Potter horn antenna should fix this.

LNB	Receiver Temperature (K)
Amiko	124.5
Amiko	129.4
Inverto	102.5
Inverto	98.2

Table 5: Hot Cold load test of the LNBs with new connector

With the LNBs mounted on the telescope, again a few fast hot cold measurements were done which yielded a stable receiver temperature lower than 100 Kelvin. The results of these tests are more elaborate described in 8.2. All the previous tests were done on both polarizations and yielded different receiver temperatures. For both LNBs the polarization where the supplied voltage is 13 V gave the lowest receiver temperature. This is the probe which lies the deepest into the waveguide, behind the polarizer bar.

8.2 Hot Cold Tests

Both for the Inverto and the Amiko LNB an aluminum flauge was made for a connection to the horn antenna. With the LNB on the horn hot cold measurements were done to determine which LNB had the lowest receiver temperature which the beam width of the horn. These tests showed that the Inverto LNB systematically had a lower receiver temperature by about 20 Kelvin. This LNB was determined to be permanent on the telescope and was glued on the aluminum flench as described in section 6. With the LNB permanent on the telescope some more advanced hot cold load tests could be done, because with this set-up nothing should be able to influence the outcomes other than the temperature of the environment. A few long hot cold test were done where the horn would switch between the hot load and cold load. For every hot load / cold load pair a receiver temperature has been calculated.

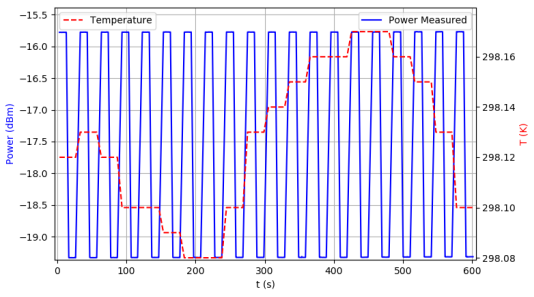

(a) Hot Cold Load measurements

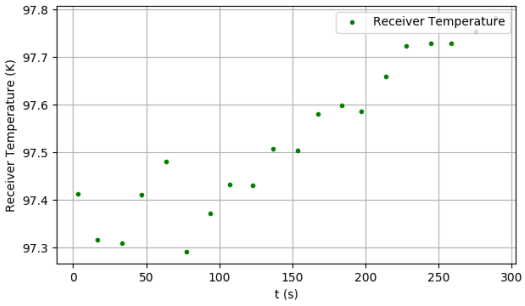

(b) Receiver Temperature per hot cold load pair.

Figure 20: Hot Cold tests of LNB on the horn.

In Figure 20 we can see one of those hot cold tests. On the left we can see the power measured versus the time. Also the temperature change of the hot load is shown. This temperature change is of the order of 0.05 Kelvin and we will consider it not to have any influence on this measurement. On the right the receiver temperature is shown versus the time. For the first 100 seconds the receiver temperature stays approximately the same, after which a small drift upwards can be seen. This drift can possibly be explained by surface reflections of the liquid nitrogen. Over the period of the test, which was 600 seconds, the distance to the liquid nitrogen could have changed, resulting in constructive or destructive reflections.

8.3 Allan Variance

First Allan Variance tests were done on June 2017. This was done in a large open lab. To test for the Allan variance there should be a stable environment for the telescope to be in. At first we thought this place was good enough for the test. Stability measurements have been taken of the hot load. For an extended amount of time the horn was facing the hot load and thus only measuring the black body of the calibrator. First results of the stability test showed that the lab was not controlled enough. In Figure 21a we can see that the temperature fluctuates a lot, and thus the read out of the system also fluctuates.

This showed that we had to move the telescope to a more controlled environment. A small room was found where we could put the telescope. After the stability test (see Figure 21b) we could see that the temperature dropped when we left the room (the hallway was warmer) and stabilized after approximately 2000 seconds. After that time the room stayed at a constant temperature, thus the only drift the system could have was its own noise. Taking a cut from Figure 21b, which is shown in Figure 22a, the Allan Variance can be calculated. This is shown in Figure 22b. We can see that the maximum observation time should be between 1 and 10 seconds. This is too short for a sky observation. Still, just as in the case of the Allan Variance of the old system [Zandvliet, 2015], the observation can be longer than these 10 seconds, because the variance is still low compared with the accuracy we are interested in.

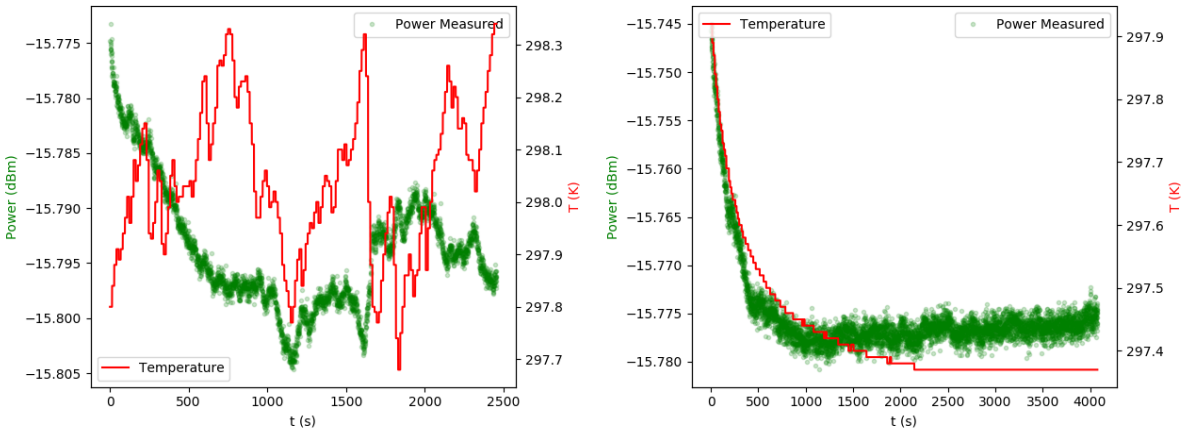

(a) Located in big lab. **(b)** Located in controlled room.

Figure 21: Stability Tests

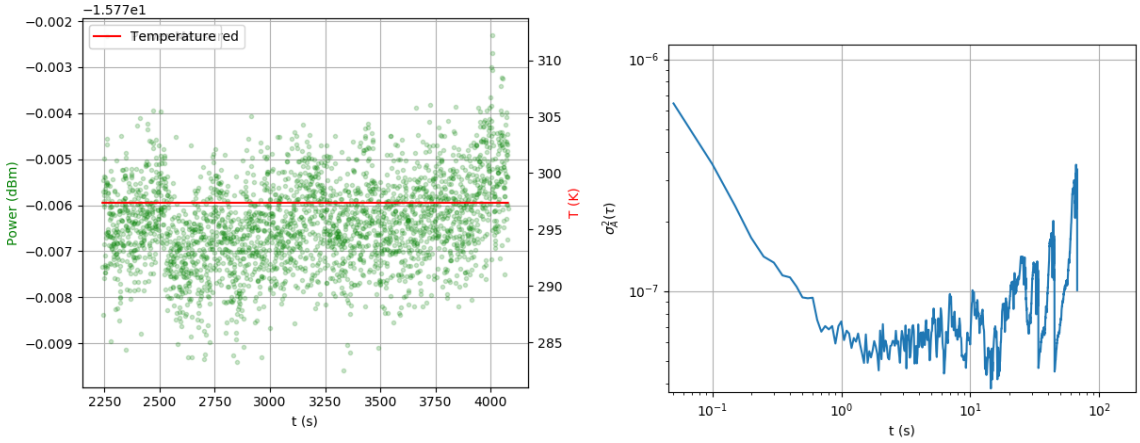

(a) Data segment of controlled room stability test. **(b)** Allan Variance of data segment.

Figure 22: Allan Variance

9 Observations

9.1 Cosmic Microwave Background

The ultimate goal is of course to measure the temperature of the CMB with the renewed telescope. When the telescope was ready for observations it was a matter of waiting for the good weather. In the evening of 21 June 2017 the sky was mostly clear of clouds, except for some high cirrus clouds. In this measurement a full calibration and sky observation could be done. The telescope was set up on the terrace of the Kapteynborg on the second floor facing south, thus the observation starts facing north going to the south horizon. Due to time constraints, a total of 2 observations were done.

Measurement	Time	Direction	Description
1	20:18	South	Sweep of the sky facing South. At start of the observation the building is in the beam. High thin clouds
2	20:26	South	Also high thin clouds

Because of the high amount of cirrus clouds, we could not get a good fit for the sky curves. This data is used to determine the half power beam width, which is described in section 9.2.

Due to the limited amount of observations done on the 21st of June, another evening of observations was scheduled on the 6th of July. This time the observations were done on top of the Bernoulliborg next to the Blaauw Observatory [6]. On this roof the telescope could point almost in every direction, making it a perfect place for observations. Due to this advantage, the telescope could be pointed to do a sweep of the sky in the Northern direction. This gives the advantage that there are no geostationary satellites in the sky, making it a perfect sky observation. Geo-stationary satellites are in the far field of the horn antenna, making them point sources. The resulting response is that of a Gaussian. This can be seen in the data as a Gaussian peak.

On the evening of the observation is was partly cloudy. A total of 18 sweeps of the sky have been made which are categorized in four series (Table. 6). The last three measurements (16,17,18) are measurements facing East with different step sizes of 1°, 5° and 1° respectively. Due to the high number of sky sweeps, they can be combined for better results. All the sky sweeps are done including calibration of the telescope, thus for every sweep the receiver temperature can be calculated. Subtracting that value from the observation gives only the sky contribution to the system temperature, thus the radiation coming from the CMB and the atmosphere.

Detailed plots of the observations can be found in the Appendix at the end of this paper. Calculating the sky curves as in section 5, the temperature of the CMB and the atmospheric opacity are calculated. Because during the observation the temperature data of the hot load and atmosphere was accidentally not saved, the uncertainties of the measurements are a bit higher than we want. The results are listed in Table 7. The uncertainty in the atmospheric temperature is chosen to be 1 Kelvin due to loss of data, but simulated data showed that if we would have known it precisely, the uncertainty would have been three times less.

[6]The Blaauw observatory is situated on top of Bernoulliborg building which houses part of the University of Groningen.

Series	Sky Measurement	Direction	Description
North 1	1,2,3,4,5	Facing Directly North	Five full sky sweeps with observation steps of 3°, partly cloudy at the start of observation.
North 2	6,7,8,9,10	Facing Directly North	Five full sky sweeps with observation steps of 2°, cloudy during first half of observation.
East 1	11,12,13,14,15	Facing 100° to East	Five full sky sweeps with observation steps of x°, a clear patch of sky from zenith to 60°.
East 2	16, 17, 18	Facing 100° to East	Various measurements.

Table 6: The measurements of July 6th categorized in four different series.

Observation	CMB Temperature	Atmospheric opacity
North1	1.71 ± 1.09 K	0.019 ± 0.003
North2	1.22 ± 1.76	0.019 ± 0.005
East1	2.16 ± 1.08	0.019 ± 0.003

Table 7: Results Observations of July 6th.

Due to clouds at zenith, the cuts made are mostly made from 10° of zenith to approximately 40°. In Figure 23 the sky pictures are shown from during the observation.

For the observations of the East 2 series the results have been calculated per sky measurement. The results of these measurements are shown in Table 8. In this table we can see that the outcome of the CMB temperature of measurement 18 is very close to the real value. In this measurement the patch of sky between zenith angle 20° and 50° was mostly free of clouds. The cut has been done in that region, giving these results. The uncertainty is still high due to loss of temperature data.

Sky Measurement	CMB Temperature	Atmospheric Opacity
16	1.67 ± 1.23	0.0198 ± 0.0005
17	3.02 ± 1.05	0.014 ± 0.002
18	2.90 ± 1.11	0.0171 ± 0.0006

Table 8: Results Observations of July 6th

(a) North, picture was taken a few minutes after observation, during observation it was similar to picture b.

(b) East

Figure 23: Sky Pictures during observations on Bernoulliborg.

9.2 Beam Width

The beam width of the telescope is determined by the transition between the horn and the waveguide. Because this transition was changed we expect that the full width half maximum of the telescope also has changed. It is important to check if this is changed, because the minimum step sizes of the sky observation are dependent on the primary beam size. First we look at the simulations made by Bram [Lap, 2015]. In this simulations he determined the best parameters for the transition and made the horn according to those outcomes. Our transition is almost the same as made by Bram, so we would not expect a big change. The parameters of the transition are listed in Table 9.

Parameter	Old Value	New Value
a_w	20 mm	19 mm
A	38 mm	38 mm

Table 9: Diameters of parameters transition of horn to waveguide. a_w is the diameter of the waveguide, A is the diameter of the horn end.

The transition we use are also modeled in the simulations by [Lap, 2015]. The beam pattern of the simulations is shown in Figure 24. The patterns shown in the figure are gathered from data from Bram Lap and expected beam width is given by Table 4 in [Lap, 2015]. These values are listed in Table 10.

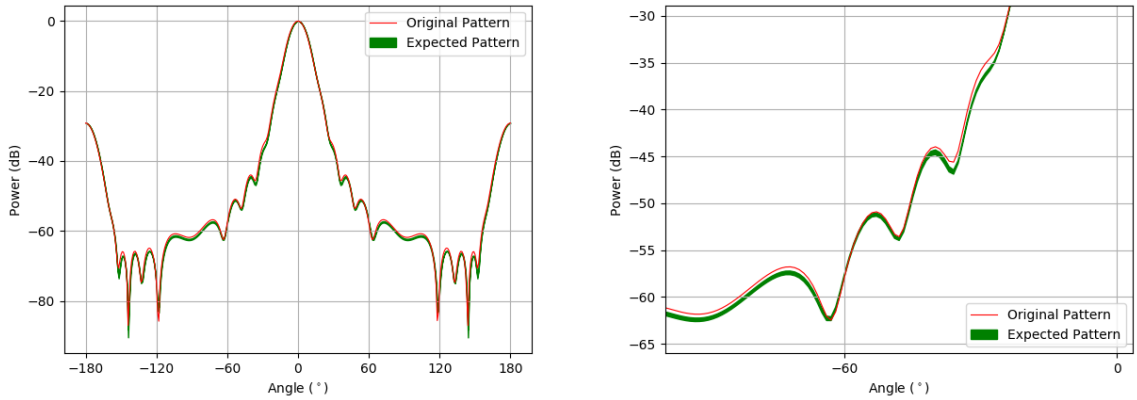

(a) Beam Patterns compared.

(b) Zoom of the patterns.

Figure 24: Simulated beam pattern of old transition and new transition

Pattern	A (mm)	a_w (mm)	FWHM (°)
58	38	18	12.89
59	38	19	12.92
60	37	20	12.86

Table 10: Simulation results of [Lap, 2015]

Given in Table 10 are the horn parameters of the simulations by Bram. Pattern 60 was the old pattern of the horn. Expected is that with the new transition, which has $a_w = 19.0$ mm, yields the beam pattern 59. Because of the inner construction of the LNB, we determined that the expected beam pattern would actually lie somewhere between pattern 58 and 59, which are shown in Figure 24. As can be seen there should not be a noticeable difference in the beam patterns, as they mostly overlap or have a really small difference.

Observations of the all the south series had a satellite in the sky curve. This satellite lies in the far field, and this can be considered as a point source. This yields in a Gaussian structure in the sky curve. With this Gaussian structure the full width half maximum (half power beam width) of the horn can now be determined. This is done by extracting the Gaussian from the sky curve. The fit to the Gaussian is shown in Figure 25. The Half Power Beam Width of this satellite Gaussian structure is determined to be 12.68 ± 0.08. This is close to the expected values of the simulations, but does not lie within the uncertainty. However, with the original setup a similar beam width of 12.61 ± 0.19 was observed [Sweijen, 2015], thus we can conclude that the beam pattern of the horn did not change.

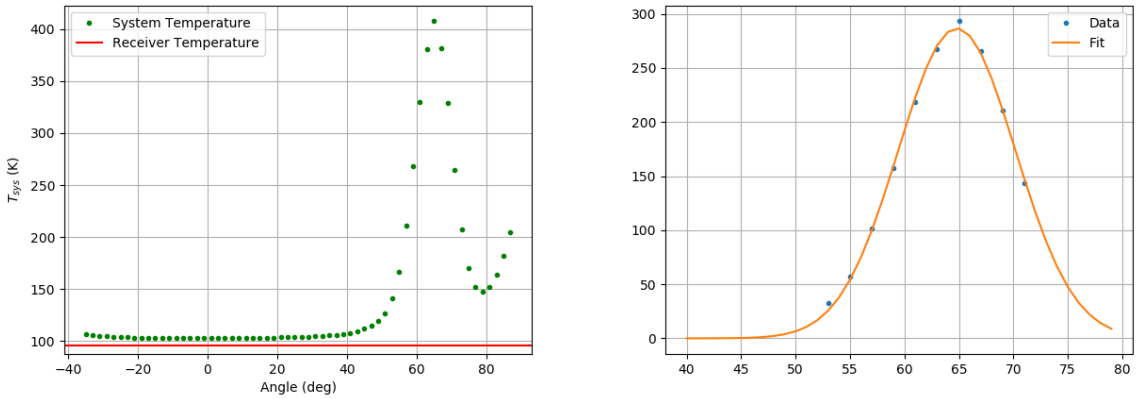

(a) Sky Observation

(b) Fit to Gaussian structure

Figure 25: Data of an observation to the South.

On the satellite band

More south observations were done to get a further understanding of the satellite band. These observations are different than the south series described above. In Figure 26 a full southern sky scan is shown. By repeatedly subtracting fits to the observed data, two Gaussian structures of satellites are found. Summing the fits of the satellites gives the purple line again, which fits exactly on the original data.

In this data set only two satellites could be recognized, but there could be more signal coming from other satellites that skew along the primary beam, or through the side lobes. The fit for Figure 26 showed a CMB temperature of -2.81 Kelvin, making us believe that due to the extra signal of satellites a sky scan of the south should be avoided.

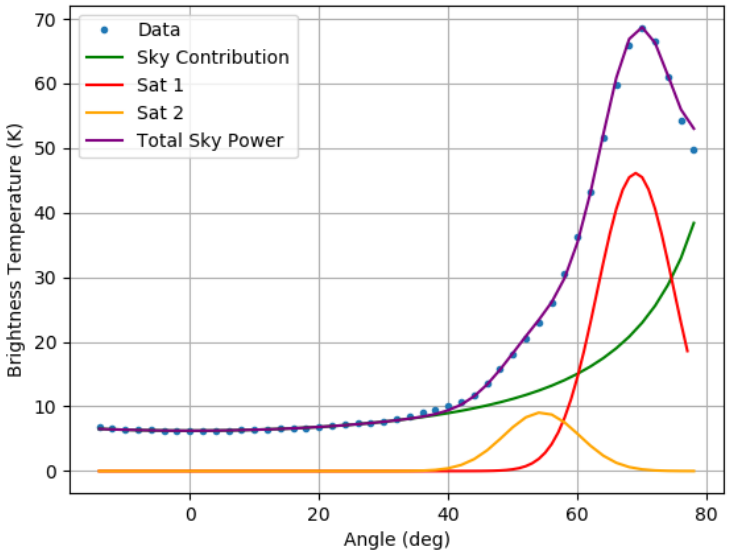

Figure 26: Satellites in the sky scan.

9.3 Sky Fluctuations

During observations the stability of the atmosphere is of great importance [Mulder, 2015]. Clouds are a big factor for the optical depth, and thus the opacity of the atmosphere. This is why we are very interested in the fluctuations of the sky opacity due to these clouds. From observations where clouds were present at zenith, curves are fitted and the residuals atmospheric opacity is calculated per zenith angle. Assumed is we can measure the CMB correctly, thus this is fixed on 2.73 Kelvin. In Figure 27 five different sky sweeps are shown that are taken in the order shown in the legend. This data is taken from the north 2 sweep as discussed in last subsection. It can be seen that later sweeps of the sky have a lower opacity. This implies that the sky became clearer during these five sweeps. However, during these observations the sky at zenith was constantly cloudy. To really get an understanding of the sky fluctuations a dedicated observation should be done where clearly is noted when clouds appear in the beam.

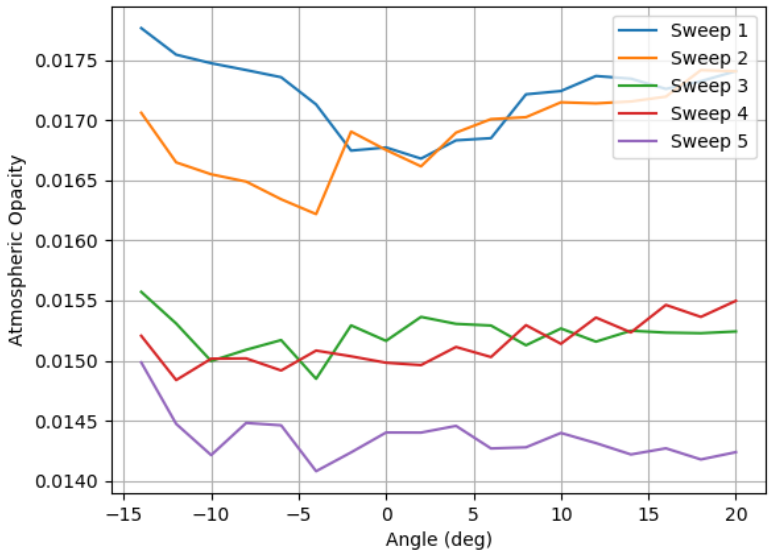

Figure 27: Atmospheric Opacities of five different sweeps performed after each other.

10 Discussion

In section 6.2 four goals were stated to be done in this project. In the discussion we will look back if those goals were achieved.

Calibration

In the original frame of the telescope, the cold load was too far from the horn antenna. The cold load did not fill the entire beam of the telescope, resulting in excess radiation coming into the telescope when measuring the cold load. The frame of the telescope was redesigned and the cold load box was replaced. The new cold load box has a large absorber area and is shielded better against stray radiation. Calibrating the telescope showed a more accurate value for the receiver noise, because the cold load could finally be measured accurately.

Upgrade of Components

The front-end components of the original telescope are replaced with an LNB. This LNB has a lower receiver temperature, making the signal to noise ratio higher. In this particular system, the receiver noise was lowered by a factor two. This gives that measurements with half of the integration time gives the same accuracy of the measurement.
The stepper motor of the system was replaced with a faster stepper motor. The old high ohmic stepper motor was controlled via voltage, while the new low ohmic motor is controlled by current. The stepper motor is upgraded along with a new stepper motor controller. This resulted in faster rotation of the horn, making the observation time of a sky scan lower. The faster the sky scan is done the more reliable the data is of the system, due to the lower Allan Variance of the system.

Sky Observation

During the project a few sky observations were done. For the first time, the KRT was not pointed to the south, but also observations pointing north were done to tackle incoming satellite signal. Observations which did not contain any satellite structure yielded better observational results than those that did. This observation made us suspect that in the south-facing observations, always extra signal is observed from the satellites in the geostationary band. This extra signal is not always seen in the data, because it can also be small fluctuations in the side lobes.

Further Improvements

When the system was ready, the sky above Groningen was not clear enough for good observations. All results in this report are with clouds in the sky which influenced the outcome. First the telescope has to be tested with a fully clear sky to see if the temperature of the CMB can accurately be determined. Also the influence of clouds should be tested with a dedicated observation. In the future the sky scan time could still be decreased by replacing the stepper motor with an even faster one. This also requires that a better stepper motor controller board has to be implemented in the system. The telescope can also be mounted on top of a rotating frame, making a full sky measurement with azimuth angle possible. This could improve the accuracy due to more data being recorded of the sky.

11 Conclusion

The objective of this Bachelor Thesis was reworking the Kapteyn Radio Telescope and perform measurements of the Cosmic Microwave Background. To accurately measure the CMB the calibration of the system needed to be improved. This was done by redesigning the telescope and making a better cold load box. The receiver system of the telescope is also altered, giving a better signal to noise ratio. This lowered the integration time, while still giving accurate measurements. Along with a upgrade of the stepper motor, the observation time could be reduced. The half power beam width of the horn was unchanged after reworking of the receiver. The half power beam width was tested by observing satellites in the far field, yielding a value of 12.68 $\pm$ 0.08, which is similar to [Sweijen, 2015]. The closest value of the temperature of the CMB was found to be 2.90 $\pm$ 1.11. More observations, when the weather is good, should give a more accurate and precise value for the temperature of the CMB. The properties of the renewed Kapteyn Radio Telescope are shown in Table 11. The full setup of the renewed KRT can be seen in Figure 28.

Property	Value
Observing Frequency	10.7 GHz - 11.7 GHz
Primary Beam Full Width Half Maximum	$12.68^\circ \pm 0.08^\circ$
Gain	67 dB
Receiver Temperature	90 - 100 K
Sky observation time	30 s

Table 11: Values for the new KRT.

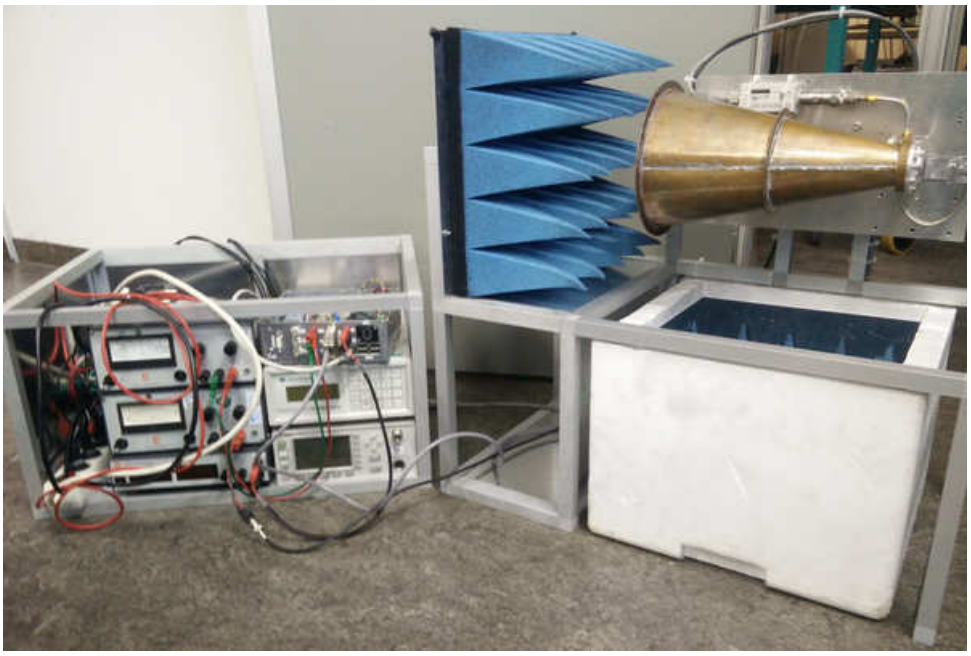

Figure 28: Kapteyn Radio Telescope with its measurement equipment.

12 Acknowledgements

I would like to thank my supervisors Andrey Baryshev and Ronald Hesper for helping me with this project, they even helped when they had no time for me. I also want to thank John McKean for setting up this project. Working on the telescope for the past two months was a great experience. In this project I had to apply the theory I learned in the past years. Learning about how the telescope works was sometimes difficult, but with the help of Bram Lap and Frits Sweijen it would always work out. I would also like to thank the people working at the workplace of SRON, for helping with constructing of the frame and flauge, especially Jarno Panman for making the flauge when nobody had the time. At last thanks to Nick Oberg for providing the LNB of his own telescope. This project could of course not be done without the support of my girlfriend, parents and fellow students of my year.

References

[Yfa, 2001] (2001). *Noise Figure, Measurement Accuracy – The Y-Factor Method*. Agilent Technologies. Application Note 57-2.

[lnb, 2010] (2010). *Single LNB, complete bias, control and power management solution*. Diodes Incorporated. DS32071 Rev. 2-5.

[Opa, 2017] (2017). Opacities zenith green bank telescope. `http://www.gb.nrao.edu/mustang/wx.shtml`. Accesses: June 2017.

[Allan, 1966] Allan, D. (1966). Statistics of Atomic Frequency Standards. *Proceedings of the IEEE*, 54:221–230.

[Alpher and Herman, 1948] Alpher, R. A. and Herman, R. C. (1948). On the Relative Abundance of the Elements. *Physical Review*, 74:1737–1742.

[Chandrasekhar, 1960] Chandrasekhar, S. (1960). *Radiative Transfer*. Dover Publications Inc.

[Fixsen, 2009] Fixsen, D. J. (2009). The Temperature of the Cosmic Microwave Background. *The Astrophysical Journal*, 707:916–920.

[Frenzel, 2013] Frenzel, L. (2013). What's The Difference Between The Third-Order Intercept And The 1-dB Compression Points? *Electronic Design*.

[Lap, 2015] Lap, B. (2015). Design of a pickett-potter horn to measure the cmb at 11 ghz.

[Lap et al., 2015] Lap, B., Mulder, W., Sweijen, F., and Zandvliet, M. (2015). *Kapteyn Radio Telescope User Manual*.

[Mulder, 2015] Mulder, W. (2015). Calibration of a 11ghz pickett-potter horn and measurements of the cosmic microwave background.

[Penzias and Wilson, 1965] Penzias, A. A. and Wilson, R. W. (1965). A Measurement of Excess Antenna Temperature at 4080 Mc/s. *The Astrophysical Journal*, 142:419–421.

[Sweijen, 2015] Sweijen, F. (2015). Computer control of a horn antenna and measuring the sun at 11 ghz.

[White, 1999] White, M., editor (1999). *Anisotropies in the CMB*.

[Wilson et al., 2013] Wilson, T., Rohlfs, K., and Huttemeister, S. (2013). *Tools of Radio Astronomy*. Springer, 6th edition.

[Zandvliet, 2015] Zandvliet, M. (2015). Back-end and mechanics of a pickett-potter horn telescope at 11ghz.

Appendix

Observational Data of July 6th

North 1 Series

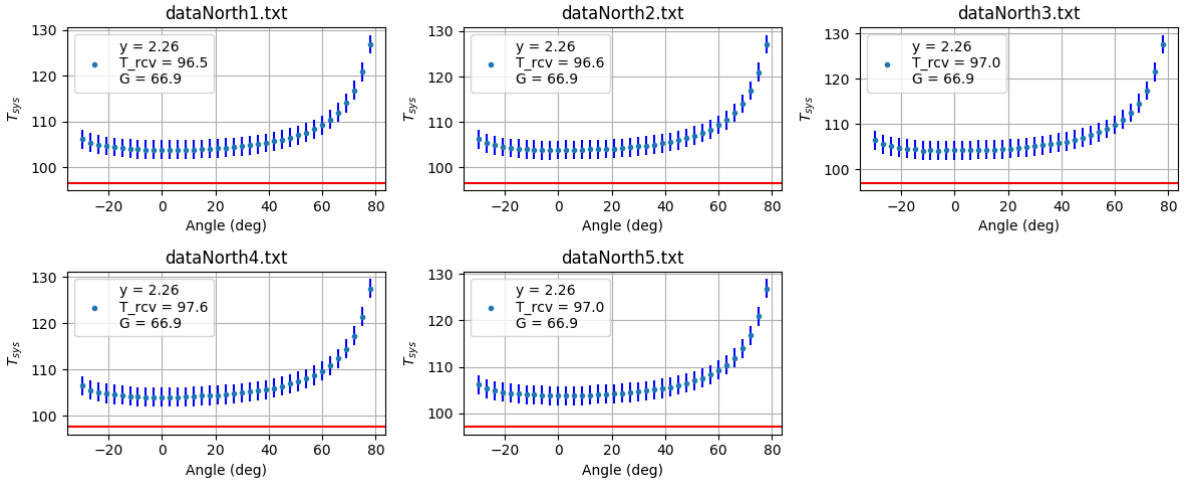

Figure 29: Data from observation, the antenna temperature of the data is plotted in blue. Along with the receiver temperature in red. In the legend is information plotted about that particular sweep.

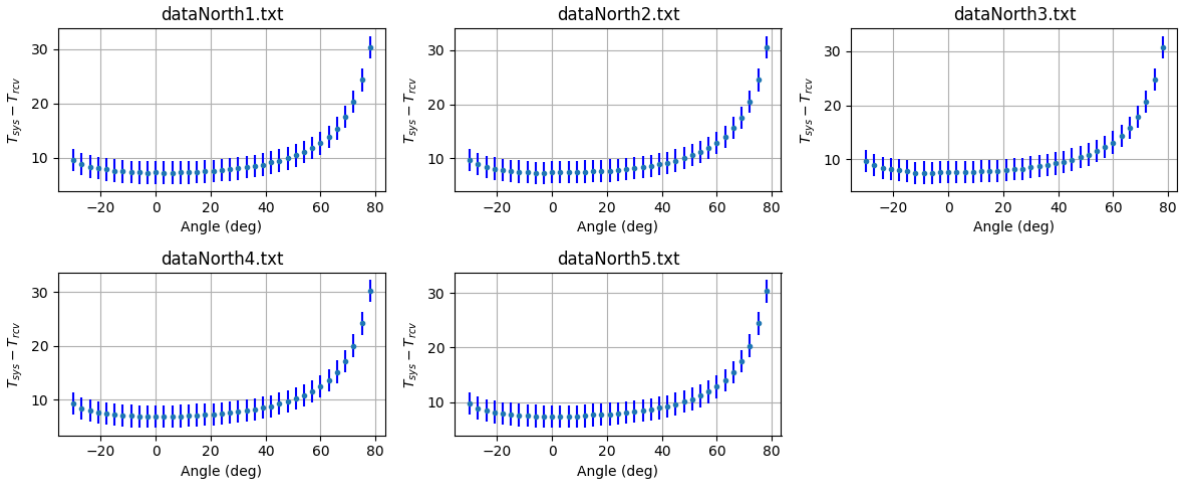

Figure 30: Receiver temperature subtracted from the data, gives only the sky contribution.

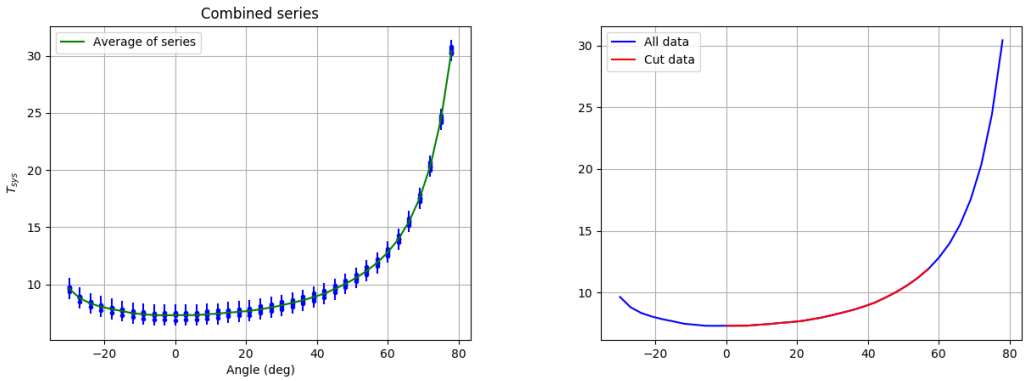

Figure 31: left: The five measurements of the series averaged to one sky curve. right: The cut in which we are interested.

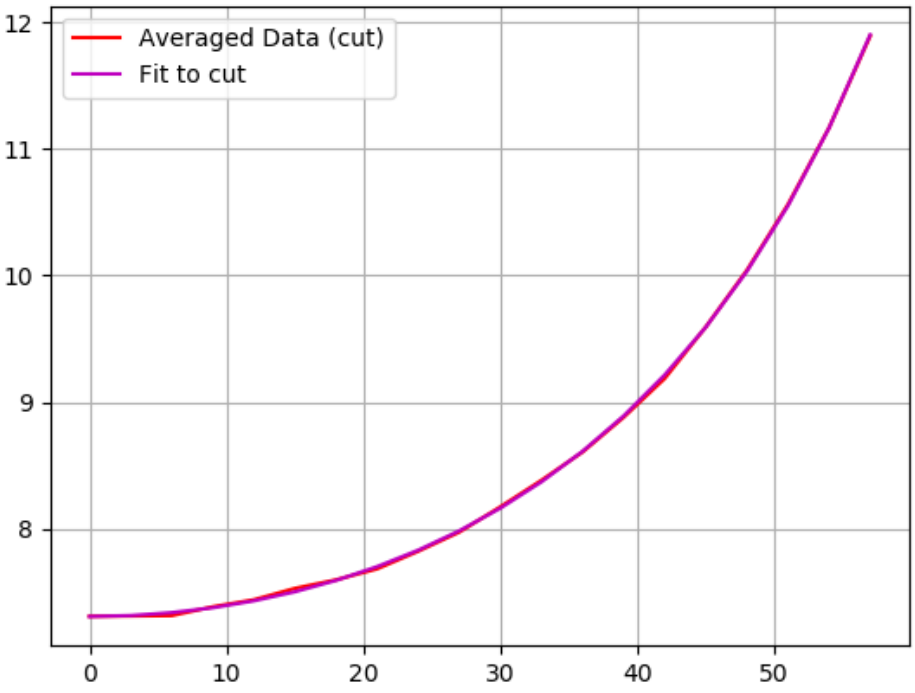

Figure 32: Fit of the sky curve

North 2 Series

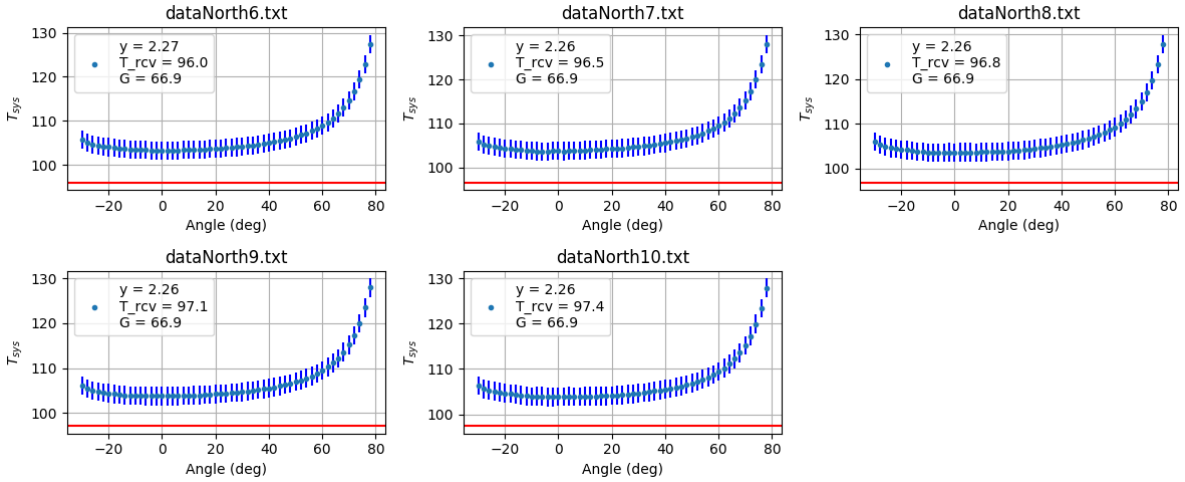

Figure 33: Data from observation, the antenna temperature of the data is plotted in blue. Along with the receiver temperature in red. In the legend is information plotted about that particular sweep.

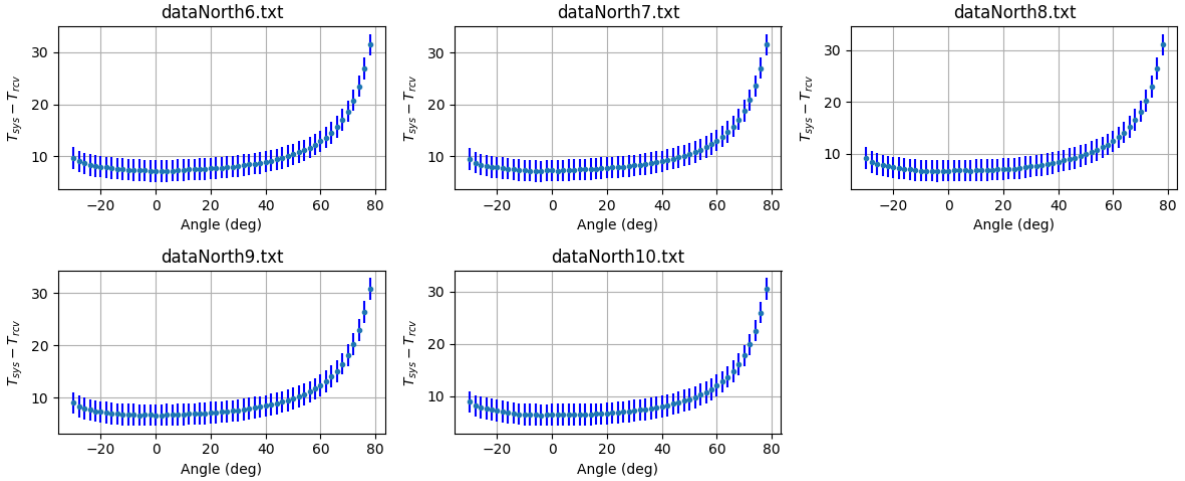

Figure 34: Receiver temperature subtracted from the data, gives only the sky contribution.

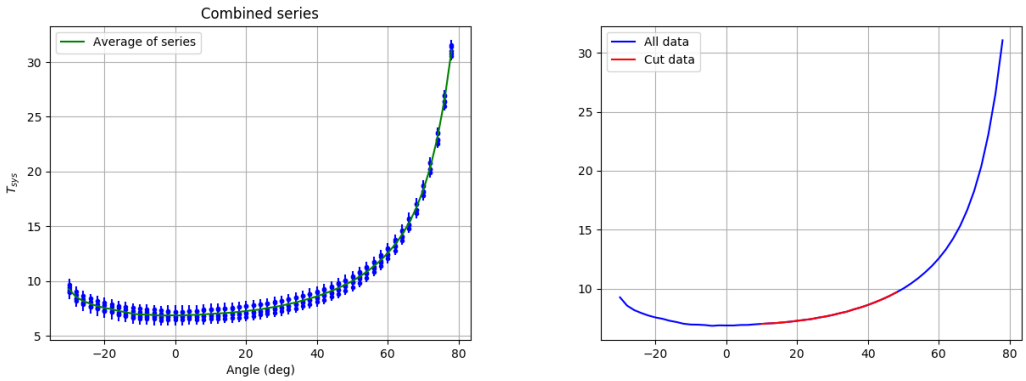

Figure 35: left: The five measurements of the series averaged to one sky curve. right: The cut in which we are interested.

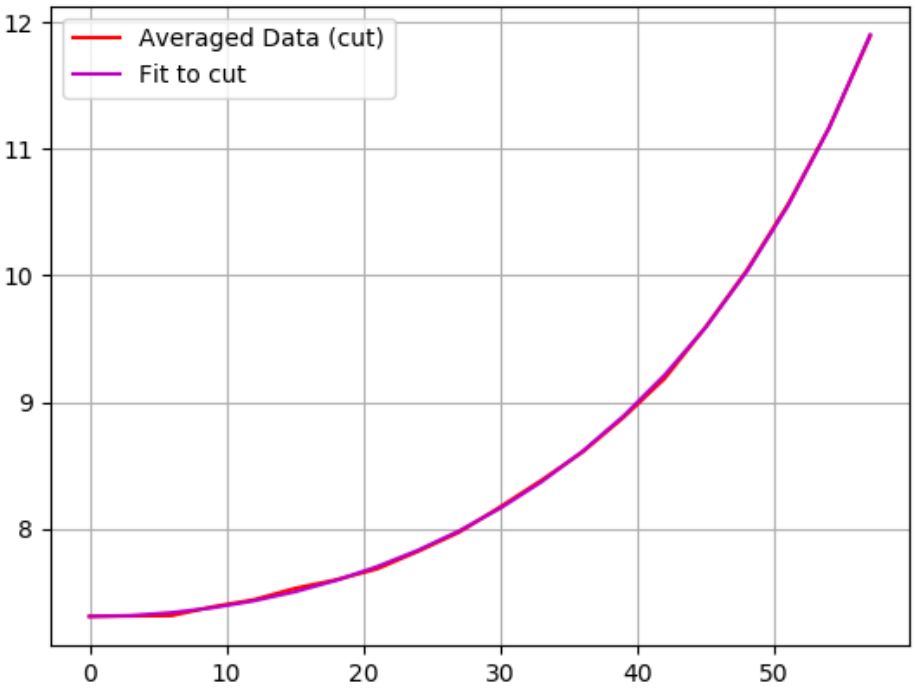

Figure 36: Fit of the sky curve

East 1 Series

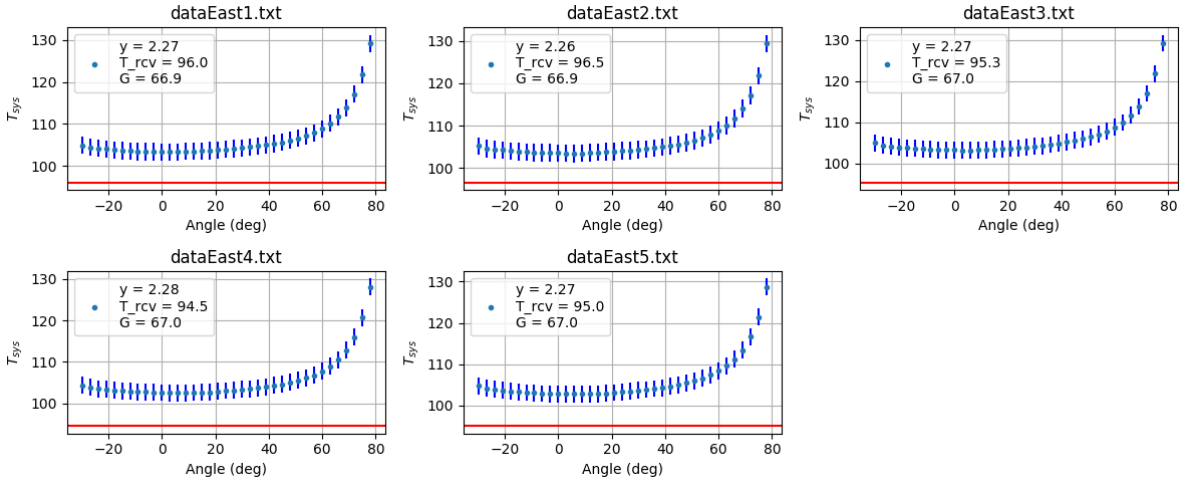

Figure 37: Data from observation, the antenna temperature of the data is plotted in blue. Along with the receiver temperature in red. In the legend is information plotted about that particular sweep.

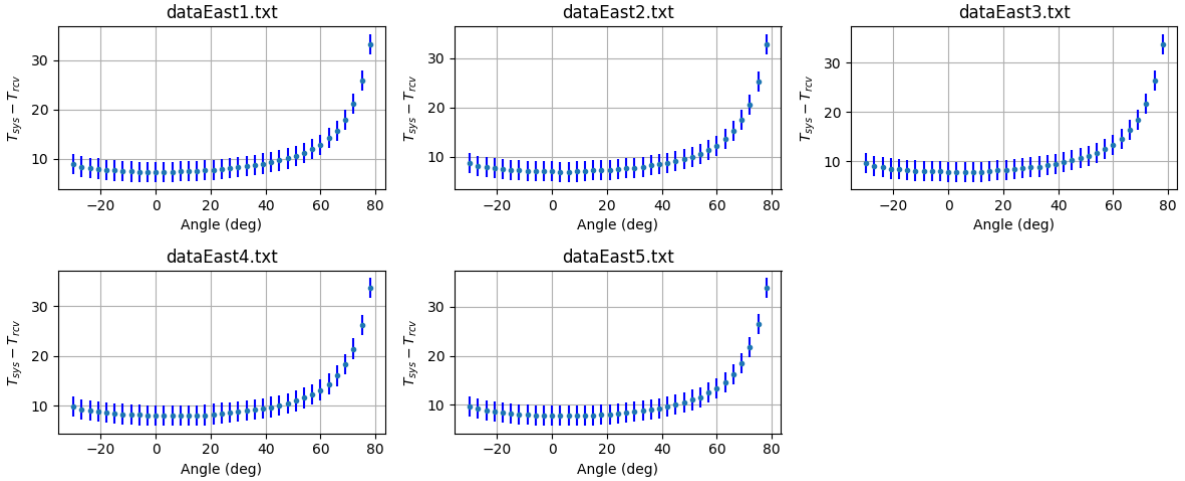

Figure 38: Receiver temperature subtracted from the data, gives only the sky contribution.

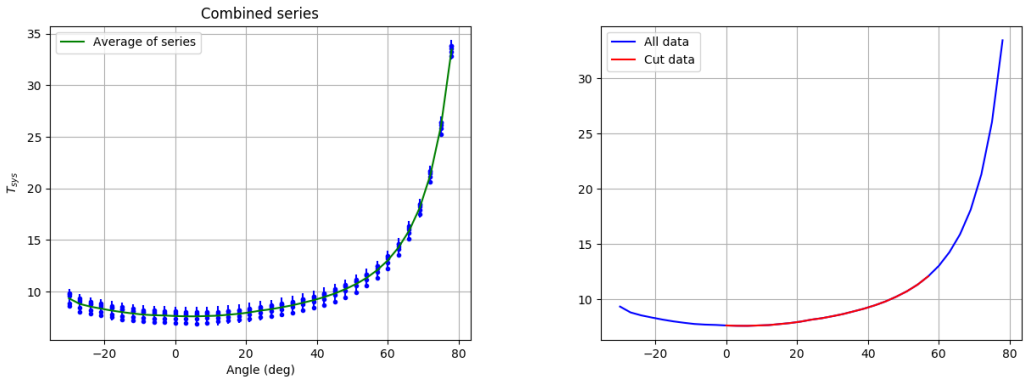

Figure 39: left: The five measurements of the series averaged to one sky curve. right: The cut in which we are interested.

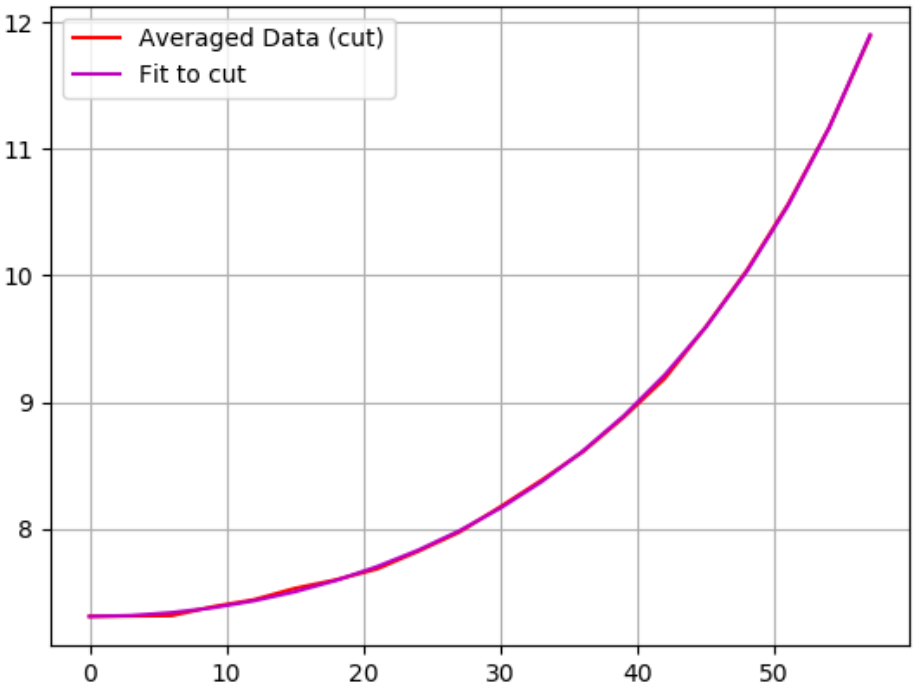

Figure 40: Fit of the sky curve

East 2 series

dataEast6

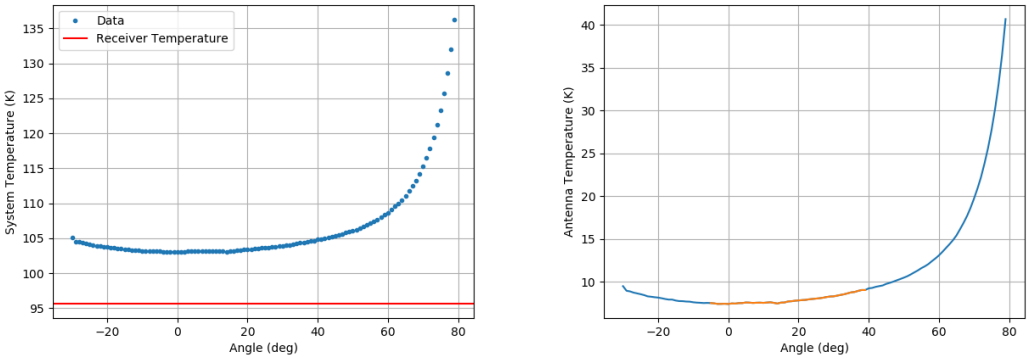

Figure 41: left: Data sky curve. right: The cut in which we are interested.

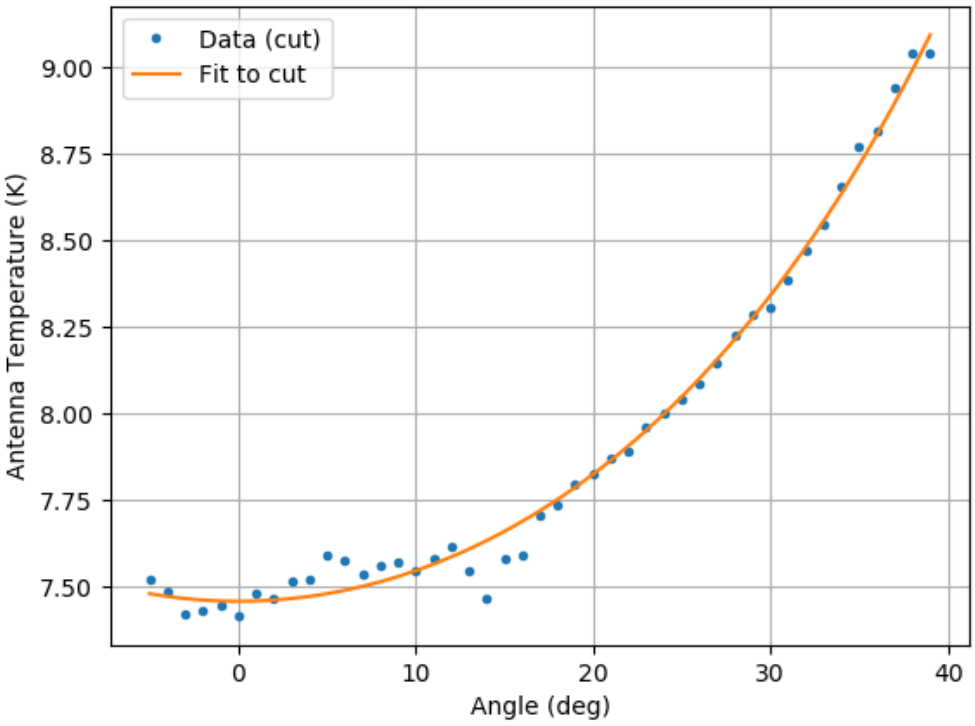

Figure 42: Fit of the sky curve

dataEast7

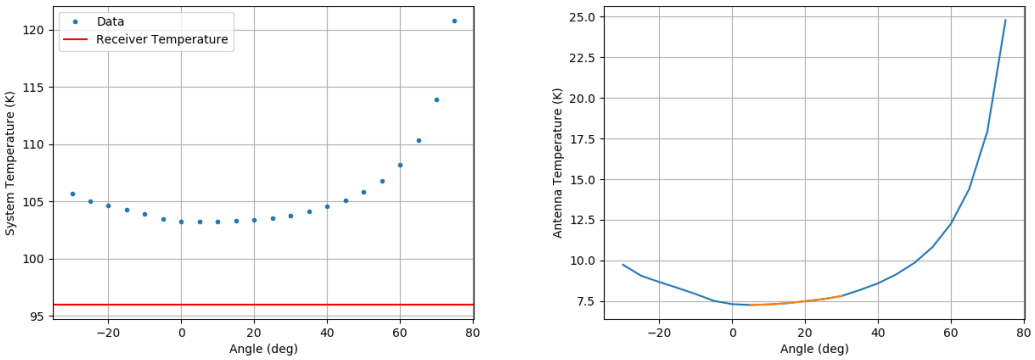

Figure 43: left: Data sky curve. right: The cut in which we are interested.

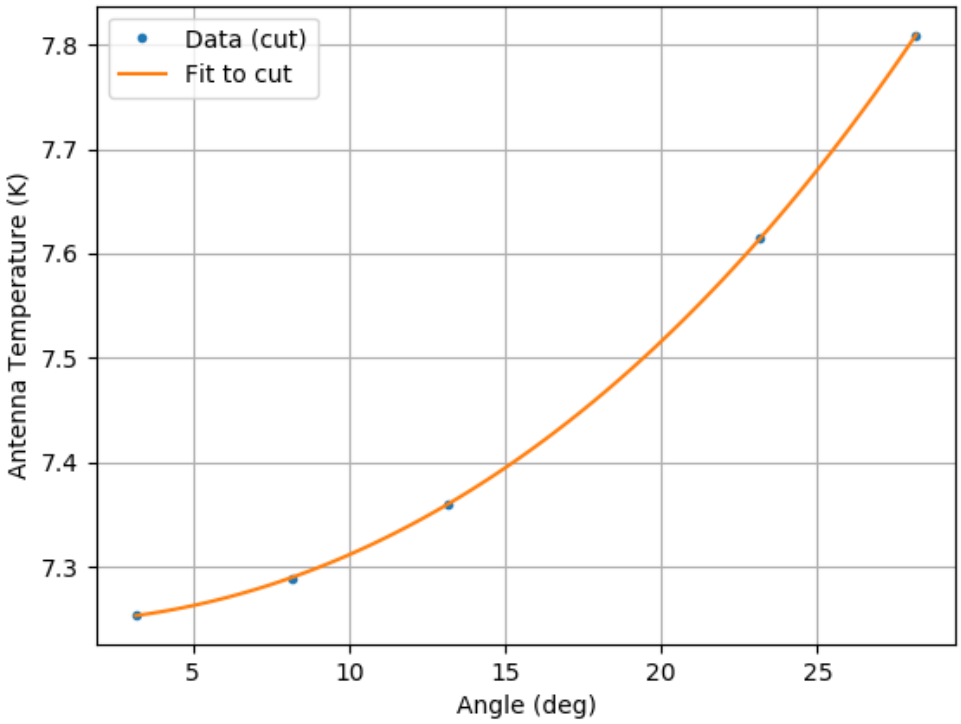

Figure 44: Fit of the sky curve

dataEast8

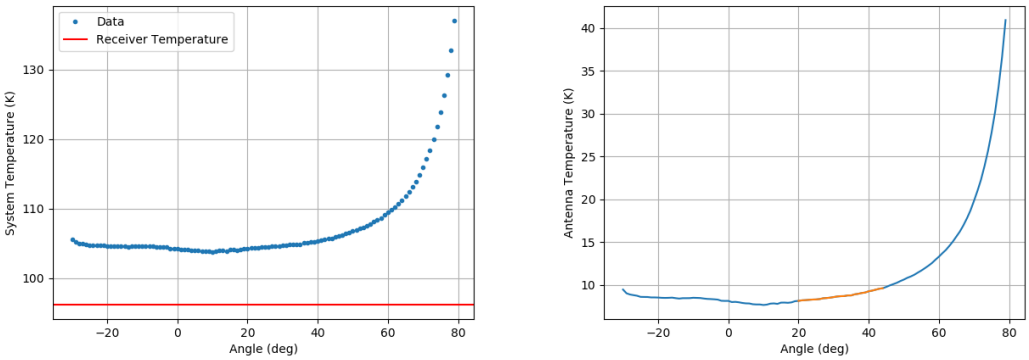

Figure 45: left: Data sky curve. right: The cut in which we are interested.

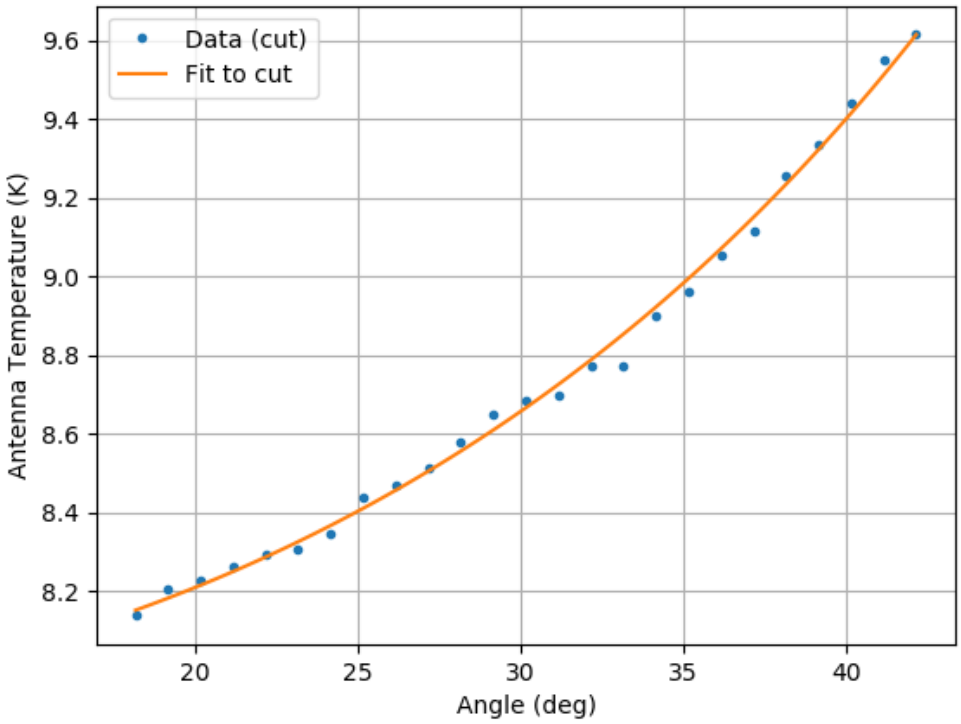

Figure 46: Fit of the sky curve